TAMPEREEN TEKNILLINEN YLIOPISTO
TAMPERE UNIVERSITY OF TECHNOLOGY

WU YUANYUAN

COMPARISON OF DIFFERENT COMMERCIAL SOLAR PHOTOVOLTAIC MODULES

Master of science thesis

Examiner: Professor Seppo Valkealahti
the examiner and topic of the thesis were approved by the Council of the Faculty of Computing and Electrical Engineering on 4th May 2016.

ABSTRACT

TAMPERE UNIVERSITY OF TECHONOLOGY
Master's Degree Programme in Electrical Engineering
WU, YUANYUAN: Comparison of different commercial solar photovoltaic modules
Master of Science Thesis, 55 pages
May 2016
Major: Smart grids
Examiner: Professor Seppo Valkealahti
Keywords: Photovoltaic module, single-diode model, I – V and P – V characteristics, comparison

Photovoltaic (PV) modules are used to convert the solar energy into practical electricity. There are some different materials which are applied to produce PV modules. The most commonly used materials include crystalline silicon, Cadmium Telluride (CdTe), Copper Indium Gallium Selenide (CIGS), and amorphous silicon (a-Si). The thesis is developed in order to compare these different PV modules.

First, the solar energy and the structure of PV module are introduced briefly in order to understand the operating principles. This thesis presents the construction of a single-diode model and its enhanced version for the PV modules, based on manufacturers' datasheets, which is in Standard Test Conditions (STC). The models are generated in Matlab Simulink software in two conditions: variation of temperature with standard irradiance, and variation of irradiance with constant temperature. The simulation results are shown in the form of Current – Voltage (I – V) and Power – Voltage (P – V) curves. The variation of short circuit current (I_{sc}) and open circuit voltage (V_{oc}) with different temperature are in good agreement with the temperature coefficients of I_{sc} and V_{oc}. When irradiance changes, the short circuit current is in proportion to insolation, while the open circuit voltage changes in logarithm relation with irradiance.

In this thesis, the PV modules which are made of different materials are compared from four perspectives: fill factor in STC, solar power efficiency in STC, power warranty and PV module stability. The first three properties can be calculated from the datasheets' parameters, while the last property is analyzed from two aspects: temperature dependence of maximum power, and irradiance dependence of maximum power, according to I – V and P – V curves. Monocrystalline silicon PV module is the most efficient, stable and longlived product, but it is very expensive. Polycrystalline silicon PV module is not so efficient and stable as monocrystalline silicon PV module, however, it is produced more simply and costs less. As for the thin film PV modules, they are so flexible and cheap that are appropriate for the situation where space is not an issue.

PREFACE

The Master of Science Thesis has been done in Tampere University of Technology, Department of Electrical Engineering. The properties of various commercial photovoltaic modules from different companies are compared based on the single-diode model. The supervisor and examiner of the thesis was Professor Seppo Valkealahti.

I would like to thank Professor Valkealahti for the interesting topic and excellent guidance and support during the process. Great thanks also to my friends Ujjwal Datta, Guo Yu, Qian Yanlin who helped me a lot with my thesis. I also benefitted from talking about the issues about writing in English with my cousin, Wu Naiyun. Finally, I especially thank my parents Xiuzhi and Chunliang for encouraging me and keeping me motivated.

Tampere, 4.5.2016

Wu Yuanyuan

Contents

ABBREVIATIONS AND NOTATION

Notation

A	Diode ideality factor
A_Z	Solar cell area
G	Irradiance
G_{STC}	Irradiance in standard test conditions
I	Current
I_{mpp}	Current in maximum power point
$I_{mpp,STC}$	Maximum power point current at standard test conditions
I_o	Saturation current of the diode in single-diode model of photovoltaic cell
I_{oc}	Open circuit current
Ir	Irradiance
I_{rec}	Current losses through recombination
I_{sc}	Short circuit current
$I_{sc,STC}$	Short circuit current at standard test conditions
k	Boltzmann constant
k_i	Temperature coefficient of short circuit current
k_v	Temperature coefficient of open circuit voltage
N_j	Number of junction in the photovoltaic cell
N_s	Number of series connected photovoltaic cells in a photovoltaic module
P	Power
P_{mpp}	Power in maximum power point
q	Electron charge
R_s	Series resistance
R_{sh}	Shunt resistance
T	Temperature
T_{STC}	Temperature at standard test conditions
V	Voltage
V_{bi}	Built-in module voltage
V_c	Built-in cell voltage of a single junction
V_{mpp}	Voltage in maximum power point
$V_{mpp,STC}$	Voltage in maximum power point at standard test conditions

V_{oc}	Open circuit voltage
$V_{oc,STC}$	Open circuit voltage at standard test conditions
V_t	Junction thermal voltage
$\mathcal{X}$	Tunable coefficient to improve the model accuracy
η_{PV}	PV module efficiency

Abbreviations

AM	Air mass
a-Si	Amorphous silicon
CdTe	Cadmium telluride
CIGS	Copper Indium Gallium Selenide
DC	Direct current
FF	Fill factor
PV	Photovoltaic
STC	Standard test conditions

1. INTRODUCTION

Both the economy and the society is developing quickly, and the energy demand is rocketing. Fossil fuels, including coal, oil, and gas, are still the main energy sources. However, the fossil fuels are not only limited but they are also causing environmental pollution and greenhouse effect. Therefore, it is necessary to develop renewable energy sources, which include wind power, hydropower, solar, bio and geothermal energy. One of these renewable energies, solar energy, is beginning to play a more and more important role in the energy supply. Nowadays, although the worldwide installed electricity capacity of photovoltaic (PV) power is increasing exponentially [1], the market share of solar energy is still very small. This motivates the research to compare the existing commercial PV modules to introduce the advantages and disadvantages of different PV modules.

PV module is the hardcore of a solar power system, and there are many factors to influence the property of PV module. Fill factor is an essential parameter to determine the efficiency of a PV module. And PV module efficiency defines the annual electricity which is converted by a PV module. Power warranty provided by the manufacturer guarantees the power output of a PV module with time going by. And the rate of change of power output with temperature and irradiance illustrates the stability of a PV module.

The first objective of this thesis is developing simulation models to discover the PV modules' characteristics. As a result, the single-diode model is designed and the necessary parameters of simulating the PV modules are extracted. The PV modules are simulated at varying temperatures and irradiances, and Current – Voltage (I – V) and Power – Voltage (P – V) curves have been obtained respectively. The main objective of the thesis is comparing the characteristics of different PV modules. The comparison is given through four aspects: fill factor, PV module efficiency and power warranty are based on datasheets, while the rate of change of power output is based on I – V and P – V curves.

The objectives will be achieved by simulating the models in Matlab and Simulink software. Single-diode model has been used to get the necessary parameters, then simulation of the model has been done in Simulink by changing temperatures and keeping irradiance at 1000 W/m^2, and changing irradiances with the fixed temperature of 25 ℃.

After acquiring the I – V and P – V curves respectively, the rate of change of power output can be obtained by comparing the stability of different PV modules.

The thesis is organized as follows. Chapter 2 discusses the technical background of PV modules. At first, the solar energy resources will be introduced briefly. The development of solar cell technology will be presented. Finally, a concise description of the construction of a solar cell and the relationship among PV cell, module, string and array will be shown. Chapter 3 introduces two simulation model for different PV modules. The single-diode model is used to model crystalline silicon, CdTe, and CIGS PV modules. The enhanced single-diode model is for amorphous silicon PV module. Both of the models are based only on manufacturers' datasheet. In Chapter 4, the simulation results of different PV modules are given by I – V and P – V curves under two conditions: different temperatures with constant irradiance and different irradiances with constant temperature. According to the curves and the datasheets, the PV modules are evaluated in Chapter 5 by comparing their fill factor, PV module efficiency, power warranty and the rate of change of power output in different conditions. Finally, the conclusion of this thesis is presented in Chapter 6 together with the topic for further future.

2. TECHNICAL BACKGROUND OF THE THESIS

The chapter introduces the technical background of the thesis topic and clarifies the incentive of the research. Firstly, a concise introduction to the solar energy resource and fuel shares of world electricity generation is presented. Subsequently, the developments of solar cell technology are given. Then the Structure of photovoltaic (PV) modules is shown jointly with the components of PV cell. Finally, the main characteristics of different cell types are discussed.

2.1 Solar Energy Resource

Solar energy is radiant light and heat that is produced by the nuclear fusion in the sun's core. It is an abundant energy source. In only one hour, the solar energy reaching the Earth is enough to satisfy the world's energy consumption for a whole year. There are two types of solar energy: thermal energy and electrical energy. Thermal systems produce heat from the sun's radiation, this can have many applications such as being a water heater. While the PV systems convert light directly into electricity by semiconductor technology.

With development of the human society, more and more energy sources are required. According to "2014 Key World Energy Statistics", 78.8% of the world electricity was generated by fossil fuels in 2012 [2]. The fossil fuels include coal, petroleum and natural gas, formed from remains of dead plants and animals by natural process. They are costly and cause amount of pollution, moreover, they are not renewable and they will be depleted one day. As a result, renewable energy, which was regarded as uneconomic sources previously, has become an applicable solution in the near future.

Solar energy is a kind of clean and renewable energy. Sun is an endless source of energy and it is free of charge. It is an environmental friendly energy without any pollution. It helps to decrease the emission of harmful gas and reduces global warming. Compared with the wind power system, solar cells are silent energy providers which do not create any noise. In addition, solar power systems can also be mounted on buildings and vehicles, due to its small size and light weight, it is not only a space-saving option but also not restricted by consumers' location.

The growth of electricity generation from renewable energy sources is primarily due to the development of the wind and solar power. Figure 2.1 presents the electricity generation from renewable energy sources and their share of consumption. It can be observed that solar energy utilization is increasing with years.

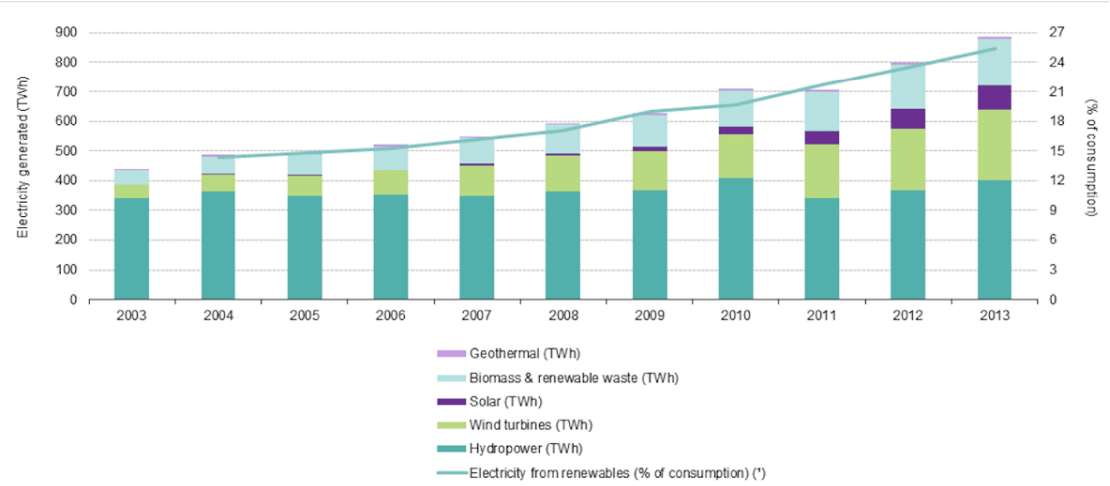

Figure 2.1 *Electricity generated from renewable energy sources, EU-28, 2003–13 [3].*

Although the production share remained relatively low, solar energy has been expanding rapidly in 10 years from 0.4 TWh in 2003 to 85.3 TWh in 2013. At the same time, the contribution of solar power of all electricity generated from renewable energy sources rose from 0.1 % to 9.6 % [3].

2.2 Developments in Solar Cell Technology

In 1839, the photovoltaic effect was firstly discovered by Alexandre Edmond Becquerel, who observed it via an electrode in a conductive solution exposed to light [4]. The phenomenon could not be understood until Albert Einstein published a paper explaining the photoelectric effect on a quantum basis in 1905 [4]. An American inventor, Charles Fritts, was the first to develop solar cells using selenium wafers to give less than 1% efficiency in 1883 [4]. 1918 marks a big year in the history since Jan Czochralski, a Polish scientist, figured out a method to grow monocrystalline silicon, his discoveries laid the foundation for solar cells based on silicon, which still constitute the major PV market until now [4]. In 1954, Bell Labs announced that the first practical silicon solar cell was invented, in other words, they made the first effective device convert sunlight into electrical power, these cells had about 6 % efficiency [4]. Hoffman Electronics later pushed the conversion efficiency from 8 % to 14 % [4]. PV cells made their debut in 1958 when they were launched into outer space on board the Vanguard Satellite [5].

In 1976, the first amorphous silicon PV cells were created with 1.1 % efficiency [4]. Four years later in 1980, the first thin film solar cell exceeding 10 % efficiency was developed [4]. Solar power has seen a huge surge in popularity as a renewable energy in recent years, largely owing to the government encouragements for example tariffs.

2.3 Structures of Photovoltaic Modules

Photovoltaic cells, the basic component of solar power systems, are a type of semiconductor device which converts sunlight into direct current (DC) electricity. They are rarely installed individually since a PV cell can only generate half a volt of electricity. The maximum current of a cell is proportional to its surface area and depends on the intensity of the sunlight [6]. Figure 2.2 shows the relationship among PV cell, PV module, PV string and PV array.

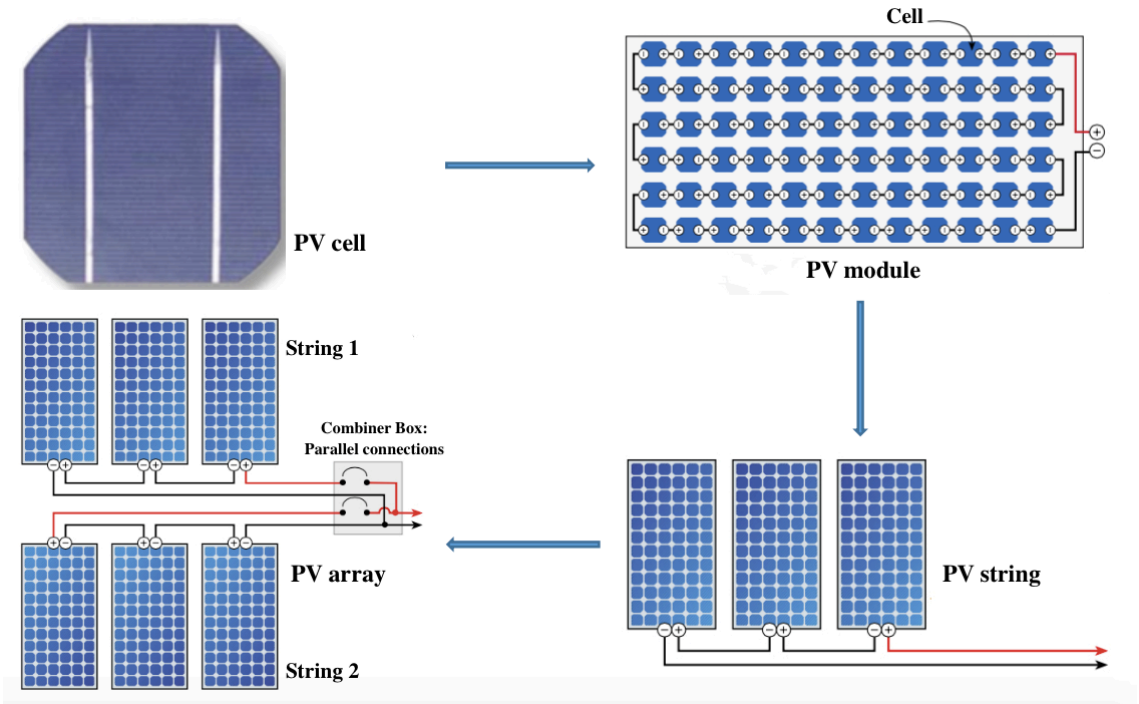

Figure 2.2 *From PV cell to PV array [6].*

PV cell materials must contain the property of sunlight absorption. The conventional PV cells are made of crystalline silicon, such as monocrystalline and polycrystalline silicon. More than 95 % solar cells are made of crystalline silicon [7]. The thin film PV cells are regarded as the second generation cells, including CdTe, CIGS and amorphous silicon solar cells. They are commonly utilized in photovoltaic power stations.

Most of the monocrystalline silicon is produced by Czochralski process. The monocrystalline silicon solar cells use the high purity raw material and cut from mono-crystal silicon ingots, so they are the most expensive cell. In 2013, the market share of monocrystalline silicon solar cells is 36 %, which ranked behind the polycrystalline silicon solar cells [8].

Polycrystalline silicon is composed of many visible small grains which are arranged irregularly. The polycrystalline silicon solar cells are made from square silicon substrates, which are cut from polycrystalline ingots or a sheet growth technique [9]. The production process is easier, cheaper, and more environmental friendly than monocrystalline silicon solar cells, although it is not so energy efficient.

Thin film PV cells consist of a semiconductor layer with a few microns thick, which is around 100 times thinner than crystalline silicon cells, thus, they are flexible and lightweight. As a result, they help open up some new applications. Most thin film PV cells are direct bandgap semiconductors. They are able to absorb the energy contained in sunlight with a much thinner layer than indirect bandgap semiconductors such as traditional crystalline silicon PV cells [10]. However, thin film PV cells just make sense in the place where space is not an issue, so it cannot be adopted by general residents widely.

PV cells are made of two different types of semiconductor materials, the construction is shown in Figure 2.3.

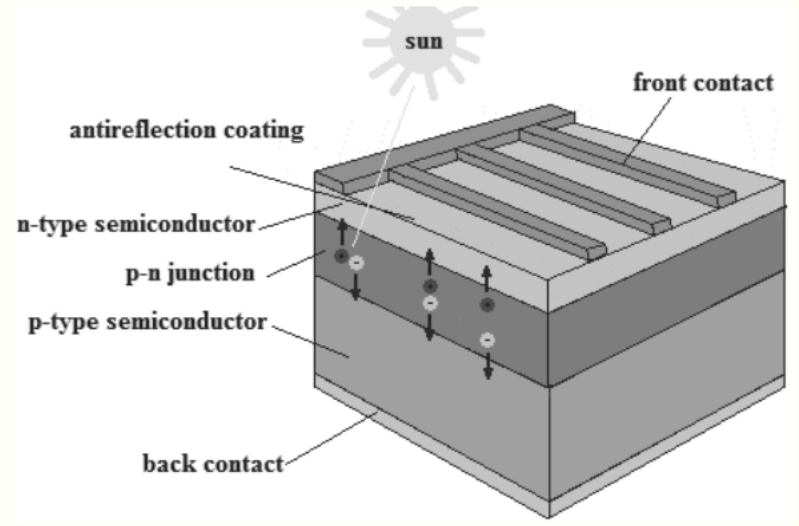

Figure 2.3 *Construction of a solar cell [11].*

Due to different electric characteristics of the materials, positive and negative charge distributions are formed on two sides of the material interface creating an electric field across the interface. When photons of sunlight are absorbed by the semiconductor materials, the photons give enough energy to break the atoms, the electrons loosed from the atoms finally end up to opposite sides of the PV cell. In order to absorb most of the solar radiation, the front contact should have proper shape [11]. By connecting PV cell surfaces to an external circuit, where a DC current is created.

PV modules composed of many PV cells are wired in parallel to produce more current and in series to get a higher voltage. PV modules with 36 PV cells are popular for large power productions [12]. PV strings consist of one or more PV modules, like in Figure 2.2, three PV modules are connected in series to constitute a PV string. The PV array describes all of the PV modules in a solar power system. These modules are wired in series or in parallel to deliver the voltage, which can be increased by increasing the number of solar cells.

3. MODELING OF THE PHOTOVOLTAIC MODULES

In order to compare the different photovoltaic (PV) modules, it is necessary to construct a model to simulate and evaluate them. There are numerous methods to model the PV modules. The well-known single-diode model is applied in this paper, since it is much more practical than the double-diode model for common tasks while more accurate than the simplified single-diode model (without shunt resistance R_{sh}). The single-diode model takes into account the nominal values provided by the Standard Test Conditions (STC), which are usual test conditions for the purpose of specifying photovoltaic cell or module guide values: irradiance 1000 $\mathrm{W/m^2}$, Air Mass 1.5 spectrum, cell temperature 25 ℃.

In addition, the single-diode model is adequately accurate for monocrystalline silicon and polycrystalline silicon PV modules, and it is also reliably applied for modeling CIGS and CdTe PV modules [13]. Whereas in case amorphous silicon (a-Si), the obtained results cannot be accepted as being credible, the additional intrinsic layer is added in the semiconductor region of a-Si PV cell.

The chapter figures out the simulation model respectively used to get the simulation results and analysis presented in Chapters 4 and 5.

3.1 Modeling of crystalline silicon, CIGS and CdTe PV modules

3.1.1 Equivalent circuit and starting equations of single-diode model

Figure 3.1 provides the equivalent circuit diagram of single-diode model, which includes four components: a photo current source, a diode parallel to the source, a series resistor R_s and a shunt resistor R_{sh}. The intensity of I_{ph} is proportional to the incident radiation. R_s models the internal losses due to current flow and the connection between cells, while R_{sh} represents the leakage current to the ground. [14]

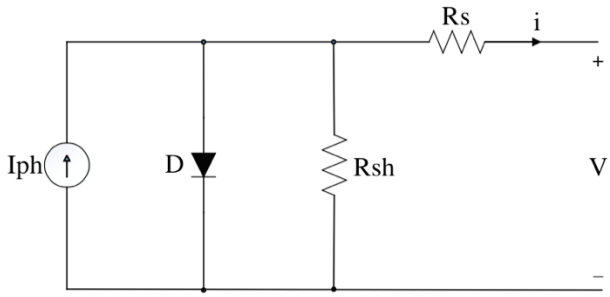

Figure 3.1 *Equivalent circuit diagram of single-diode model of a PV cell*

.

The expression for the current *I* as a function of voltage *V* of a PV module based on the single-diode model is:

$$I = I_{ph} - I_o(e^{\frac{V+I\,R_s}{A\,V_t}} - 1) - \frac{V + IR_s}{R_{sh}} \quad (1)$$

In the above equation, V_t is the junction thermal voltage:

$$V_t = \frac{N_s k T_{STC}}{q} \quad (2)$$

Where:

- I_{ph} is the photo-generated current in STC
- I_o is dark saturation current in STC
- R_s is series resistance
- R_{sh} is parallel (shunt) resistance
- A is diode ideality factor

I_{ph}, I_o, R_s, R_{sh} and A are the five parameters of the model, while k is Boltzmann's constant ($1.381 \cdot 10^{-23}$ J/K), q is the electron charge ($1.602 \cdot 10^{-19}\ C$), N_s is the number of cells in the module connected in series, and T_{STC} ($°K$) is the temperature at STC. It is a common practice to neglect the term '-1' in Eq. (1), due to in silicon devices, the dark saturation current is very small compared to the exponential term since V_t is very small [1].

In order to construct an electrical model of a PV module, we have to find the parameters of I_{ph}, I_o, R_s, and R_{sh} without any measurements by using only the data from datasheet. Meanwhile, $A = 1.2$ is assumed for crystalline silicon modules [15], while $A = 1.5$ is used for CdTe and CIGS thin film PV modules [16].

The I – V characteristic of PV module is based on three key points: the short-circuit point, the maximum power point, and the open-circuit point. These points are measured by the manufacturers in STC.

At short circuit condition, *V=0*, so that Eq. (1) can be written as:

$$I_{sc} = I_{ph} - I_o(e^{\frac{I_{sc}\,R_s}{AV_t}} - 1) - \frac{I_{sc}R_s}{R_{sh}} \quad (3)$$

At the maximum power point condition, $V = V_{mpp}$ and $I = I_{mpp}$, so that Eq. (1) can be written as:

$$I_{mpp} = I_{ph} - I_o(e^{\frac{V_{mpp} + I_{mpp}\,R_s}{AV_t}} - 1) - \frac{V_{mpp} + I_{mpp}\,R_s}{R_{sh}} \quad (4)$$

At open circuit condition, *I=0*, so that Eq. (1) can be written as:

$$I_{oc} = 0 = I_{ph} - I_o(e^{\frac{V_{oc}}{AV_t}} - 1) - \frac{V_{oc}}{R_{sh}} \quad (5)$$

Where:

- I_{sc} is short circuit current in STC
- V_{oc} is open circuit voltage in STC
- V_{mpp} is voltage at the Maximum Power Point (MPP) in STC
- I_{mpp} is current at the MPP in STC
- P_{mpp} is power at the MPP in STC

The above parameters are normally provided by the manufacturer's datasheet.

At the MPP given by the manufacturer, the derivative of power is zero because of $P = VI$,

$$\left.\frac{dP}{dV}\right|_{\substack{V=V_{mpp} \\ I=I_{mpp}}} = 0 \quad (6)$$

3.1.2 Parameter Extraction of single-diode model

According to the current at open-circuit conditions, the photo-generated current I_{ph} can be expressed based on Eq. (5)

$$I_{ph} = I_o(e^{\frac{V_{oc}}{AV_t}} - 1) + \frac{V_{oc}}{R_{sh}} \quad (7)$$

Insert Eq. (7) into Eq. (3), we can get I_{sc}

$$\begin{aligned} I_{sc} &= I_o(e^{\frac{V_{oc}}{AV_t}} - 1) + \frac{V_{oc}}{R_{sh}} - I_o(e^{\frac{I_{sc}R_s}{AV_t}} - 1) - \frac{I_{sc}R_s}{R_{sh}} \\ &= I_o\left(e^{\frac{V_{oc}}{AV_t}} - e^{\frac{I_{sc}R_s}{AV_t}}\right) + \frac{V_{oc} - I_{sc}R_s}{R_{sh}} \end{aligned} \quad (8)$$

R_s is very small, and $I_{sc}R_s$ is smaller than V_{oc}, so $e^{\frac{I_{sc}R_s}{AV_t}}$ is much smaller than $e^{\frac{V_{oc}}{AV_t}}$ and can be omitted, so it takes the form:

$$I_{sc} = I_o e^{\frac{V_{oc}}{AV_t}} + \frac{V_{oc} - I_{sc}R_s}{R_{sh}} \quad (9)$$

We can get the dark saturation current I_o from Eq. (9),

$$I_o = \left(I_{sc} - \frac{V_{oc} - I_{sc}R_s}{R_{sh}}\right) e^{-\frac{V_{oc}}{AV_t}} \quad (10)$$

Insert Eq. (7) and (10) into Eq. (4),

$$\begin{aligned} I_{mpp} = I_o\left(e^{\frac{V_{oc}}{AV_t}} - 1\right) + \frac{V_{oc}}{R_{sh}} - \left(I_{sc} - \frac{V_{oc} - I_{sc}R_s}{R_{sh}}\right) e^{-\frac{V_{oc}}{AV_t}}(e^{\frac{V_{mpp} + I_{mpp}R_s}{AV_t}} - 1) \\ - \frac{V_{mpp} + I_{mpp}R_s}{R_{sh}} \end{aligned}$$

According to Eq. (9), $I_o e^{\frac{V_{oc}}{AV_t}}$ can be substituted by $I_{sc} - \frac{V_{oc} - I_{sc}R_s}{R_{sh}}$, then the above equation just contains two parameters R_s and R_{sh}.

$$I_{mpp} = \left(I_{sc} - \frac{V_{oc} - I_{sc}R_s}{R_{sh}}\right) e^{-\frac{V_{oc}}{AV_t}} \left(e^{\frac{V_{oc}}{AV_t}} - 1\right) - \frac{V_{mpp} + I_{mpp}\,R_s - V_{oc}}{R_{sh}}$$

$$- \left(I_{sc} - \frac{V_{oc} - I_{sc}\,R_s}{R_{sh}}\right) (e^{\frac{V_{mpp} + I_{mpp}\,R_s - V_{oc}}{AV_t}} - e^{-\frac{V_{oc}}{AV_t}})$$

So,

$$I_{mpp} = I_{sc} - \frac{V_{mpp} + I_{mpp}\,R_s - I_{sc}\,R_s}{R_{sh}} - \left(I_{sc} - \frac{V_{oc} - I_{sc}\,R_s}{R_{sh}}\right) e^{\frac{V_{mpp} + I_{mpp}\,R_s - V_{oc}}{AV_t}} \quad (11)$$

In order to calculate the unknown derivatives: R_s and R_{sh}. The derivative of the power with voltage at MPP can be written as:

$$\frac{dP}{dV} = \frac{d(IV)}{dV} = I + \frac{dI}{dV}V \quad (12)$$

In order to obtain the derivative of the power at MPP, the derivative of I_{mpp} with voltage should be found. Express Eq. (11) as the following form:

$$I = f(I, V) \quad (13)$$

The $f\ (I, V)$ should be right side of Eq. (11), differential equation of Eq. (13):

$$dI = dI\ \frac{\partial f(I,V)}{\partial I} + dV\ \frac{\partial f(I,V)}{\partial V} \quad (14)$$

The derivative of the current with voltage:

$$\frac{dI}{dV} = \frac{\frac{\partial}{\partial V} f(I,V)}{1 - \frac{\partial}{\partial I} f(I,V)} \quad (15)$$

Insert Eq. (15) into Eq. (12):

$$\frac{dP}{dV} = I + \frac{V\frac{\partial}{\partial V}f(I,V)}{1-\frac{\partial}{\partial I}f(I,V)} \tag{16}$$

So

$$\left.\frac{dP}{dV}\right|_{\substack{V=V_{mpp}\\I=I_{mpp}}} = 0 = I_{mpp} + V_{mpp}\frac{-\frac{(I_{sc}R_{sh}-V_{oc}+I_{sc}R_s)e^{\frac{V_{mpp}+I_{mpp}R_s-V_{oc}}{AV_t}}}{A\,V_t\,R_{sh}} - \frac{1}{R_{sh}}}{1+\frac{R_s(I_{sc}R_{sh}-V_{oc}+I_{sc}R_s)e^{\frac{V_{mpp}+I_{mpp}R_s-V_{oc}}{AV_t}}}{A\,V_t\,R_{sh}} + \frac{R_s}{R_{sh}}} \tag{17}$$

R_s is inside and outside of the exponential term, so we will not be able to obtain an analytic expression for R_s. However, we can obtain two different expressions for R_{sh} as a function of R_s only according to Eq. (11) and (17) and then iteratively solve them.

$$R_{sh1} = \frac{V_{mpp} + I_{mpp}R_s - I_{sc}R_s + (I_{sc}R_s - V_{oc})e^{\frac{V_{mpp}+I_{mpp}R_s-V_{oc}}{AV_t}}}{I_{sc}\left(1-e^{\frac{V_{mpp}+I_{mpp}R_s-V_{oc}}{AV_t}}\right) - I_{mpp}} \tag{18}$$

$$R_{sh2} = \frac{(V_{mpp}-I_{mpp}R_s)((I_{sc}R_s - V_{oc})e^{\frac{V_{mpp}+I_{mpp}R_s-V_{oc}}{AV_t}} + AV_t)}{I_{mpp}AV_t + I_{sc}\left(I_{mpp}R_s - V_{mpp}\right)e^{\frac{V_{mpp}+I_{mpp}R_s-V_{oc}}{AV_t}}} \tag{19}$$

It is possible now to determine R_s and R_{sh} using Eq. (18) and (19). Then we can get I_{ph} and I_o according to Eq. (7) and Eq. (10).

3.2 Modeling of amorphous silicon PV modules

3.2.1 Enhanced equivalent circuit and starting equations

The equivalent circuit diagram of enhanced single-diode model is shown in Figure 3.2. A current sink is added to the singe-diode model presented in Subchapter 3.1.1, since the intense recombination losses in an amorphous silicon PV cell cannot be described by the

single-diode model [17].

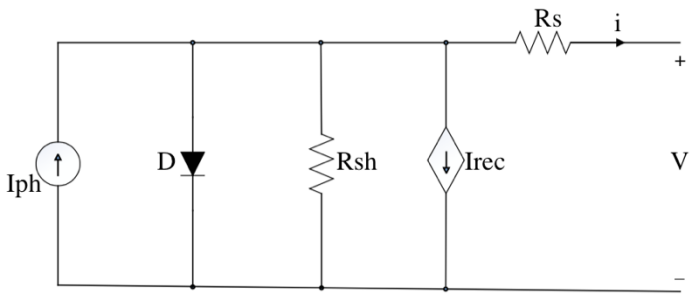

Figure 3.2 *Equivalent circuit diagram of enhanced single-diode model of a PV cell.*

The general current-voltage characteristic of amorphous silicon solar cell based on the enhanced single-diode model is:

$$I = I_{ph} - I_o\left(e^{\frac{V+I\,R_s}{A\,V_t}} - 1\right) - \frac{V + IR_s}{R_{sh}} - I_{rec} \qquad (20)$$

In the above equation, V_t is the junction thermal voltage, I_{rec} represents current losses through recombination:

$$V_t = \frac{N_s k T_{STC}}{q}$$
$$I_{rec} = \frac{\mathcal{X} I_{ph}}{V_{bi} - (V + IR_s)} \qquad (21)$$

The built-in module voltage $V_{bi} = N_s N_j V_c$, where $\mathrm{V_c}$ is the built-in cell voltage of a single junction, N_j is the number of junction in the cell, and N_s is the number of cell in series [17]. N_j and N_s are provided by the PV manufacturers while $V_c = 0.88\,V$ is assumed for a-Si p-i-n junction cells [18]. The model is insensitive to V_{bi}, which had less influence on the other operating points [19]. The $\mathcal{X}$ coefficient, corresponding to a voltage value, depends on the intrinsic layer thickness (d_i), which is usually an unknown parameter [17]. As a result, $\mathcal{X}$ is extracted by a fitting procedure, which maximizes the matching between the I – V curve and the model, so that $\mathcal{X}$ is no longer considered as an unknown parameter but as a tunable coefficient used to improve the model accuracy [17]. $\mathcal{X} = 6.07\ \mathrm{V}$ is used for a two layers amorphous silicon PV modules [19].

In order to construct an electrical model of a PV module, we have to find the parameters

of I_{ph}, I_o, R_s, and R_{sh} without any measurements by using only the data from datasheet. Meanwhile, $A = 2$ is assumed for a-Si:H solar cells [20]. Eq. (20) can be written for the three key points of V – I characteristic: the short-circuit point, the maximum power point, and the open-circuit point.

At short circuit condition, *V=0*, so that Eq. (20) can be written as:

$$I_{sc} = I_{ph} - I_o(e^{\frac{I_{sc}R_s}{AV_t}} - 1) - \frac{I_{sc}R_s}{R_{sh}} - \frac{\mathcal{X}I_{ph}}{V_{bi} - I_{sc}R_s} \quad (22)$$

At the maximum power point condition, $V = V_{mpp}$ and $I = I_{mpp}$, so that Eq. (20) can be written as:

$$I_{mpp} = I_{ph} - I_o(e^{\frac{V_{mpp} + I_{mpp}R_s}{AV_t}} - 1) - \frac{V_{mpp} + I_{mpp}R_s}{R_{sh}} - \frac{\mathcal{X}I_{ph}}{V_{bi} - (V_{mpp} + I_{mpp}R_s)} \quad (23)$$

At open circuit condition, *I=0*, so that Eq. (20) can be written as:

$$I_{oc} = 0 = I_{ph} - I_o(e^{\frac{V_{oc}}{AV_t}} - 1) - \frac{V_{oc}}{R_{sh}} - \frac{\mathcal{X}I_{ph}}{V_{bi} - V_{oc}} \quad (24)$$

3.2.2 Parameter extraction of enhanced single-diode model

The series resistance represents the effect of the internal resistance and cells contacts. The shunt resistance, connected in parallel with the diode, is used for representing the leakage current flowing through the crystal. R_s should be as small as possible, and R_{sh} should be as large as possible. So we assume $R_{sh} \to \infty$ and $R_s = 0$, which are inserted into Eq. (22) then we can get

$$I_{sc} = I_{ph} - \frac{\mathcal{X}I_{ph}}{V_{bi}} \quad (25)$$

The dark saturation current is very small compared to the exponential term since V_t is very small, so the term '-1' in Eq. (24) can be neglected, associating with $R_{sh} \to \infty$ then the Eq. (24) can be expressed as:

$$I_{oc} = 0 = I_{ph} - I_o e^{\frac{V_{oc}}{AV_t}} - \frac{\mathcal{X} I_{ph}}{V_{bi} - V_{oc}} \quad (26)$$

Now we can obtain I_{ph} and A according to Eq. (25) and (26),

$$I_{ph} = I_{sc} \frac{V_{bi}}{V_{bi} - \mathcal{X}} \quad (27)$$

$$I_o = \frac{I_{ph}\left(\frac{V_{bi} - V_{oc} - \mathcal{X}}{V_{bi} - V_{oc}}\right) - \frac{V_{oc}}{R_{sh}}}{e^{\frac{V_{oc}}{AV_t}} - 1} \quad (28)$$

At the MPP given by the manufacturer, the derivative of power is zero since $P = VI$, so

$$\left.\frac{dP}{dV}\right|_{\substack{V=V_{mpp} \\ I=I_{mpp}}} = 0 \quad (29)$$

The derivative of the power with voltage at MPP can be written as:

$$\frac{dP}{dV} = \frac{d(IV)}{dV} = I + \frac{dI}{dV} V \quad (30)$$

In order to obtain the derivative of the power at MPP, the derivative of I_{mpp} with voltage should be found. Express Eq. (23) as:

$$I = f(I, V) \quad (31)$$

Differential equation of Eq. (31):

$$dI = dI \frac{\partial f(I,V)}{\partial I} + dV \frac{\partial f(I,V)}{\partial V} \quad (32)$$

The derivative of the current with voltage:

$$\frac{dI}{dV} = \frac{\frac{\partial}{\partial V} f(I,V)}{1 - \frac{\partial}{\partial I} f(I,V)} \quad (33)$$

Insert Eq. (33) into Eq. (30):

$$\frac{dP}{dV} = I + \frac{V \frac{\partial}{\partial V} f(I,V)}{1 - \frac{\partial}{\partial I} f(I,V)} \quad (34)$$

According to Eq. (29),

$$\left.\frac{dP}{dV}\right|_{\substack{V=V_{mpp} \\ I=I_{mpp}}} = I_{mpp} + \frac{V_{mpp} \frac{\partial}{\partial V} f(I,V)}{1 - \frac{\partial}{\partial I} f(I,V)} = 0 \quad (35)$$

So

$$\begin{aligned} \frac{I_{mpp}}{V_{mpp}} &= -\frac{\frac{\partial}{\partial V} f(I,V)}{1 - \frac{\partial}{\partial I} f(I,V)} \\ &= -\frac{-\frac{I_o e^{\frac{V_{mpp} + I_{mpp} R_s}{AV_t}}}{A V_t} - \frac{\mathcal{X} I_{ph}}{(V_{bi} - V_{mpp} - I_{mpp} R_s)^2} - \frac{1}{R_{sh}}}{1 + \frac{R_s I_o e^{\frac{V_{mpp} + I_{mpp} R_s}{AV_t}}}{A V_t} + \frac{R_s}{R_{sh}} + \frac{R_s \mathcal{X} I_{ph}}{(V_{bi} - V_{mpp} - I_{mpp} R_s)^2}} \end{aligned} \quad (36)$$

Assume an intermediate variable *x,*

$$x = \frac{V_{mpp} + I_{mpp} R_s}{AV_t} \quad (37)$$

So the Eq. (36) can be simplified as:

$$\frac{I_{mpp}}{V_{mpp}} = -\frac{-\frac{I_o e^x}{A V_t} - \frac{\mathcal{X} I_{ph}}{(V_{bi} - xAV_t)^2} - \frac{1}{R_{sh}}}{1 + \frac{R_s I_o e^x}{A V_t} + \frac{R_s}{R_{sh}} + \frac{R_s \mathcal{X} I_{ph}}{(V_{bi} - xAV_t)^2}} \quad (38)$$

Then we can use the variable x to express R_s and R_{sh}

$$R_s = \frac{xA\,V_t - V_{mpp}}{I_{mpp}}$$
$$R_{sh} = \frac{xAV_t}{I_{ph} - I_{mpp} - I_o(e^x - 1) - \frac{\mathcal{X} I_{ph}}{V_{bi} - xAV_t}} \quad (39)$$

Insert Eq. (39) into Eq. (38):

$$\frac{I_{mpp}}{V_{mpp}} = -\frac{-\frac{I_o e^x}{A\,V_t} - \frac{I^*}{xA\,V_t} - \frac{\mathcal{X} I_{ph}}{(V_{bi} - xAV_t)^2}}{1 + \frac{xA\,V_t - V_{mpp}}{A\,V_t I_{mpp}}\left(I_o e^x + \frac{I^*}{x} + \frac{\mathcal{X} A\,V_t I_{ph}}{(V_{bi} - xAV_t)^2}\right)} \quad (40)$$

Where

$$I^* = I_{ph} - I_{mpp} - I_o(e^x - 1) - \frac{\mathcal{X} I_{ph}}{V_{bi} - xAV_t} \quad (41)$$

According to Eq. (37),

$$xAV_t = V_{mpp} + I_{mpp} R_s \quad (42)$$

Since R_s is very small, we can get the simplified expression of Eq. (42),

$$xAV_t = V_{mpp} \quad (43)$$

As a result, $(V_{bi} - xAV_t)^2$ can be substituted as:

$$(V_{bi} - xAV_t)^2 = \left(V_{bi} - V_{mpp}\right)^2 \quad (44)$$

According to Eq. (40), (41) and (44),

$$I_{mpp} + \left(x - \frac{V_{mpp}}{AV_t}\right)\left(I_o e^x + \frac{I^*}{x} + \frac{\mathcal{X} A\, V_t I_{ph}}{\left(V_{bi} - V_{mpp}\right)^2}\right) = \frac{I_o V_{mpp}}{A\, V_t} e^x + \frac{I^* V_{mpp}}{xA\, V_t} + \frac{\mathcal{X} I_{ph} V_{mpp}}{\left(V_{bi} - V_{mpp}\right)^2} \quad (45)$$

The Eq. (41) is simplified as

$$I^* = I_{ph} - I_{mpp} - I_o(e^x - 1) - \frac{\mathcal{X} I_{ph}}{V_{bi} - V_{mpp}}$$

Simplify Eq. (45) as following procedure:

$$I_{mpp} + I_o x e^x + I^* + \frac{\mathcal{X} A\, V_t I_{ph}}{\left(V_{bi} - V_{mpp}\right)^2} x - \frac{2 I_o V_{mpp}}{A\, V_t} e^x - \frac{2 I^* V_{mpp}}{xA\, V_t} - \frac{2\mathcal{X} I_{ph} V_{mpp}}{\left(V_{bi} - V_{mpp}\right)^2} = 0$$

According to Eq. (43), $x = \frac{V_{mpp}}{AV_t}$, so

$$I_{mpp} + \frac{I_o V_{mpp}}{A\, V_t} e^x + I^* + \frac{\mathcal{X} V_{mpp} I_{ph}}{\left(V_{bi} - V_{mpp}\right)^2} - \frac{2 I_o V_{mpp}}{A\, V_t} e^x - 2I^* - \frac{2\mathcal{X} I_{ph} V_{mpp}}{\left(V_{bi} - V_{mpp}\right)^2} = 0$$

Reorder and combine of like terms

$$I_{mpp} - I^* - \frac{I_o V_{mpp}}{A\, V_t} e^x - \frac{\mathcal{X} I_{ph} V_{mpp}}{\left(V_{bi} - V_{mpp}\right)^2} = 0$$

Insert Eq. (41) into above equation

$$I_{mpp} - \left(I_{ph} - I_{mpp} - I_o e^x + I_o - \frac{\mathcal{X} I_{ph}}{V_{bi} - V_{mpp}}\right) - \frac{I_o V_{mpp}}{A\, V_t} e^x - \frac{\mathcal{X} I_{ph} V_{mpp}}{\left(V_{bi} - V_{mpp}\right)^2} = 0$$

Transpose and combine of like terms

$$2I_{mpp} - I_{ph} - I_o + \frac{\mathcal{X} I_{ph}}{V_{bi} - V_{mpp}} - \frac{\mathcal{X} I_{ph} V_{mpp}}{\left(V_{bi} - V_{mpp}\right)^2} = \frac{I_o V_{mpp}}{A\, V_t} e^x - I_o e^x$$

So

$$x = \ln\left(\frac{2I_{mpp} - I_{ph} - I_o + \mathcal{X} I_{ph}\left(\frac{1}{V_{bi} - V_{mpp}} - \frac{V_{mpp}}{\left(V_{bi} - V_{mpp}\right)^2}\right)}{I_o\left(\frac{V_{mpp}}{AV_t} - 1\right)}\right) \qquad (46)$$

The value obtained by Eq. (46) is substituted in Eq. (39), so that the values of the series and parallel resistances result.

4. SIMULATION RESULTS OF DIFFERENT PV MODULES

The environment has a considerable influence on the performance of photovoltaic (PV) modules, such as temperature, solar radiance, wind speed and direction, and snow shading. The effect of temperature and radiance will be discussed in the thesis.

The equations in Chapter 3 are derived in STC. To include the effects of the environment, like temperature and irradiance, these equations should be completed with the corresponding terms [14].

Considering the effects of irradiance and temperature, the short circuit current can be approximated as

$$I_{sc}(G,T) = I_{sc,STC}\frac{G}{G_{STC}} + k_i(T - T_{STC}) \quad (47)$$

where k_i is the temperature coefficient of the short circuit current.

The open circuit voltage can be computed as

$$V_{oc}(G,T) = V_{oc,STC} + V_t \ln\left(\frac{G}{G_{STC}}\right) + k_v(T - T_{STC}) \quad (48)$$

where k_v is the temperature coefficient of the open circuit voltage.

The variations of the current and voltage at the maximum power point are described as:

$$I_{mpp}(G,T) = I_{mpp,STC}\frac{G}{G_{STC}} + k_i(T - T_{STC}) \quad (49)$$

$$V_{mpp}(G,T) = V_{mpp,STC} + V_t \ln\left(\frac{G}{G_{STC}}\right) + k_v(T - T_{STC}) \quad (50)$$

As a result, the maximum power point also changes as a function of temperature and irradiance. The environment dependencies will be proved by Current – Voltage (I – V) and Power – Voltage (P – V) figures.

4.1 Simulation results of crystalline silicon PV modules

The parameters used in simulations can be calculated by the method which are introduced in Subchapter 3.1.1, and then the I – V and P – V curves of crystalline silicon PV modules are acquired through simulating the single-diode model.

4.1.1 Simulation results of monocrystalline silicon PV module

The useful parameters of monocrystalline silicon PV module X21-345 from SunPower Corporation in the simulation are shown in Table 4.1 [21]. R_s and R_{sh} are calculated according to single-diode model, and the other parameters are got from manufacturer's datasheet.

Table 4.1 *Input data of X21-345 (monocrystalline) PV module to the model.*

Parameter	Value	Parameter	Value
V_{oc}	68.2 V	k_v	-167.4 mV/℃
I_{sc}	6.39 A	k_i	3.5 mA/℃
V_{mpp}	57.3 V	R_{sh}	1144.1 Ω
I_{mpp}	6.02 A	R_s	0.3429 Ω
P_{mpp}	345 W	A	1.2

In order to show the influence of temperature on the performance of monocrystalline silicon PV module, the irradiance is maintained as 1000 W/m^2. The temperature dependencies of the monocrystalline silicon PV module I – V and P – V characteristics have been verified by plotting for four different temperatures.

In Figure 4.1, the simulation results for the I – V curves change with different temperatures (0 ℃, 25 ℃, 50 ℃ and 75 ℃) and fixed irradiance 1000 W/m^2. The short circuit current and open circuit voltage at 25 ℃ are consistent with the datasheet values very well. The changes in the short circuit current and open circuit voltage also coincide

with the current and voltage temperature coefficients given in the datasheet. For example, the temperature coefficients of open circuit voltage and short circuit current are -167.4 mV/℃ and 3.5 mA/℃. As a result, the variations of open circuit voltage and short circuit current when the temperature changes from 0 ℃ to 25 ℃ should be 4.19 V and 0.088 A. In Figure 4.1, the open circuit voltages at 0 ℃ and 25 ℃ are 72.39 V and 68.2 V respectively, so the difference is 4.19 V, same as the value which is calculated by the voltage temperature coefficients. Similarly, the short circuit current at 0 ℃ and 25 ℃ are 6.302 A and 6.39 A, so the difference is 0.088 A, same as the value calculated before.

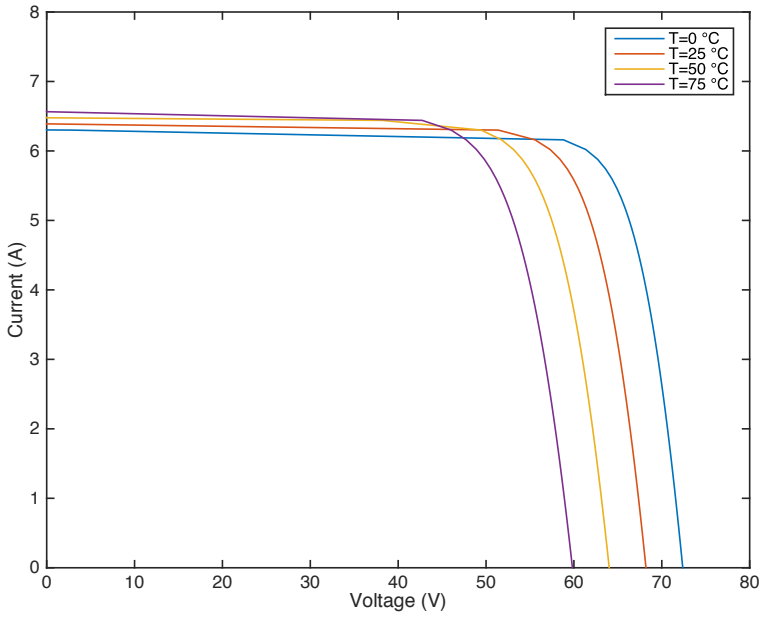

Figure 4.1 *Current-Voltage characteristic of X21-345 (monocrystalline) PV module at different temperatures and standard irradiance.*

Figure 4.2 show the variation of the power output with temperature, the value of the maximum power at 25 ℃ is 345 W, in accordance with the datasheet. Although the current at maximum power point increases slightly when the temperature increases, the maximum power point voltage clearly decreases. As a result, the maximum power clearly decreases as the cell temperature rises.

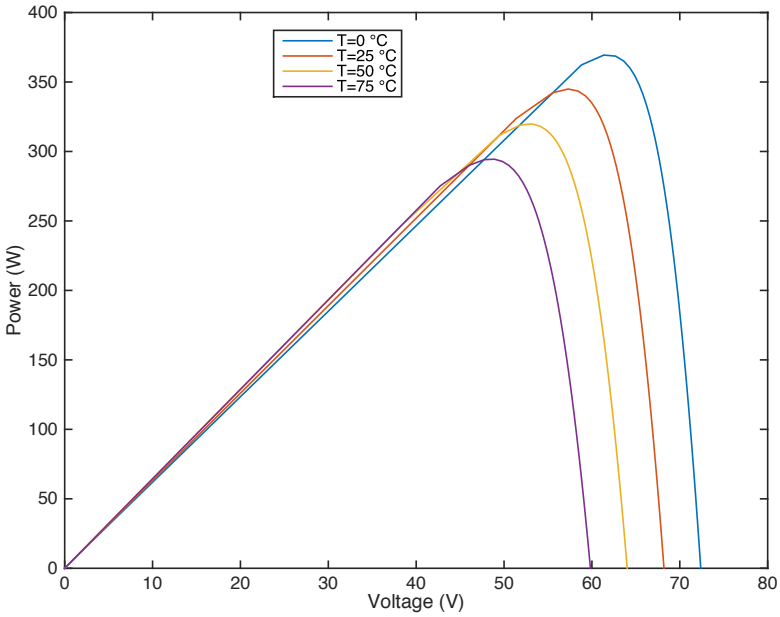

Figure 4.2 *Power-Voltage characteristic of X21-345 (monocrystalline) PV module at different temperatures and standard irradiance.*

Accordingly, aimed at describing the I – V and P – V characteristics of monocrystalline silicon PV module X21-345 with the irradiance changes, the temperature should be fixed at 25 ℃ while the irradiance changes from 200 W/m^2 to 1200 W/m^2.

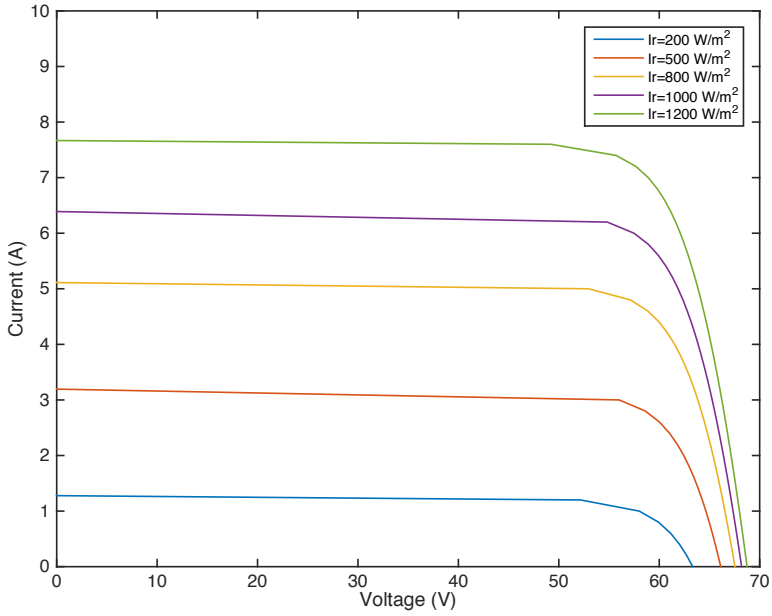

Figure 4.3 *Current-Voltage characteristic of X21-345 (monocrystalline) PV module at different irradiances and standard temperature.*

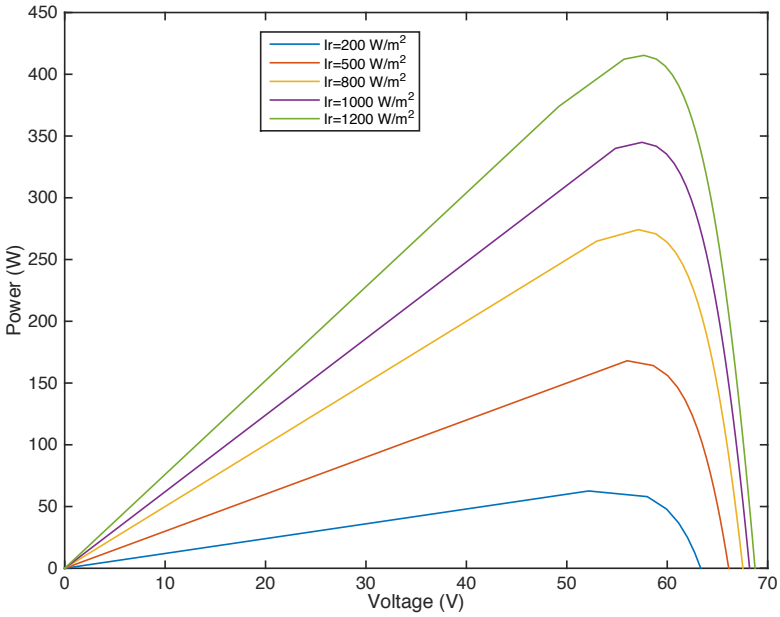

Figure 4.4 *Power-Voltage characteristic of X21-345 (monocrystalline) PV module at different irradiances and standard temperature.*

Figure 4.3 and Figure 4.4 indicate that the open circuit voltage, short circuit current and power output increase as the irradiance values increase. The variation of short circuit current of the cell is in proportion to irradiance change, as shown in Eq. (47), which can be proved by comparing the short circuit current under the irradiance of 500 W/m^2 and 1000 W/m^2: the short circuit current is equal to 3.195 A when the irradiance is 500 W/m^2, and the current changes to 6.39 A, double of 3.195 A, when the irradiance increases to 1000 W/m^2. The influence of irradiance on the open circuit voltage is smaller than on the short circuit current, because the open circuit voltage is logarithmically dependent on the irradiance, as presented in Eq. (48).

4.1.2 Simulation results of polycrystalline silicon PV module

Table 4.2 lists the input parameters of polycrystalline silicon PV module KC200GT from Kyocera Corporation [22]. Most of these parameters are from the manufacturer's datasheet and the values of R_s and R_{sh} calculated by the method introduced in section 3.1.1.

Table 4.2 *Input data of KC200GT (polycrystalline) PV module to the model.*

Parameter	Value	Parameter	Value
V_{oc}	32.9 V	k_v	-123 mV/℃
I_{sc}	8.21 A	k_i	3.18 mA/℃
V_{mpp}	26.3 V	R_{sh}	312.8 Ω
I_{mpp}	7.61 A	R_s	0.2647 Ω
P_{mpp}	200 W	A	1.2

Just like the monocrystalline silicon PV module, the temperature dependencies of the polycrystalline silicon PV module have been shown through depicting I – V and P – V curves at four temperatures from 0 ℃ to 75 ℃, the curves are given in Figures 4.5 and 4.6.

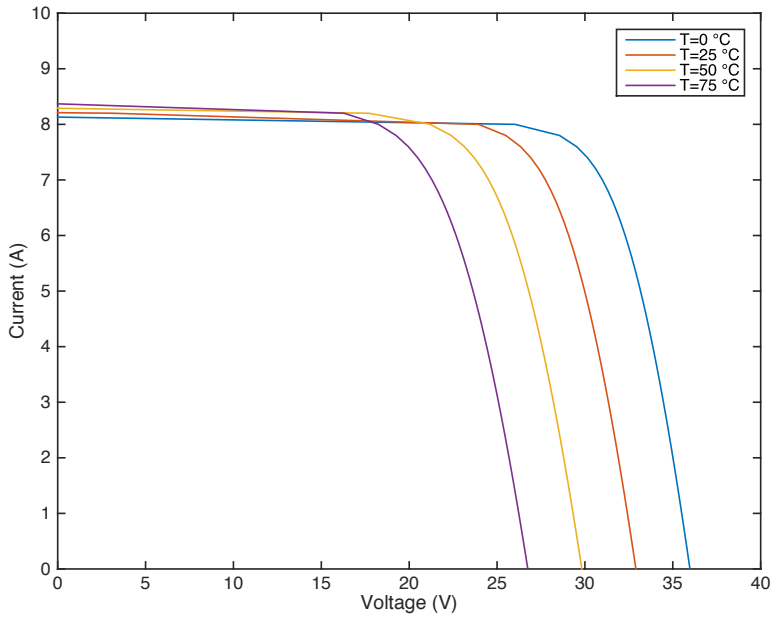

Figure 4.5 *Current-Voltage characteristic of KC200GT (polycrystalline) PV module at different temperatures and standard irradiance.*

The open circuit voltages are respectively 35.98 V, 32.9 V, 29.83 V and 26.75V when the temperatures are 0 ℃, 25 ℃, 50 ℃ and 75 ℃, the difference of open circuit voltage is 3.08 V when the temperature differs by 25 ℃. As a result, the temperature effect on open circuit voltage is -0.123 mV/℃, it is same as the temperature coefficient given in the manufacturer's datasheet. As for short circuit current, it increases 0.0795 A when the temperature increases 25 ℃. The short circuit current increases slightly with increasing temperature since the temperature coefficient of short circuit current is much smaller than

the temperature coefficient of open circuit voltage.

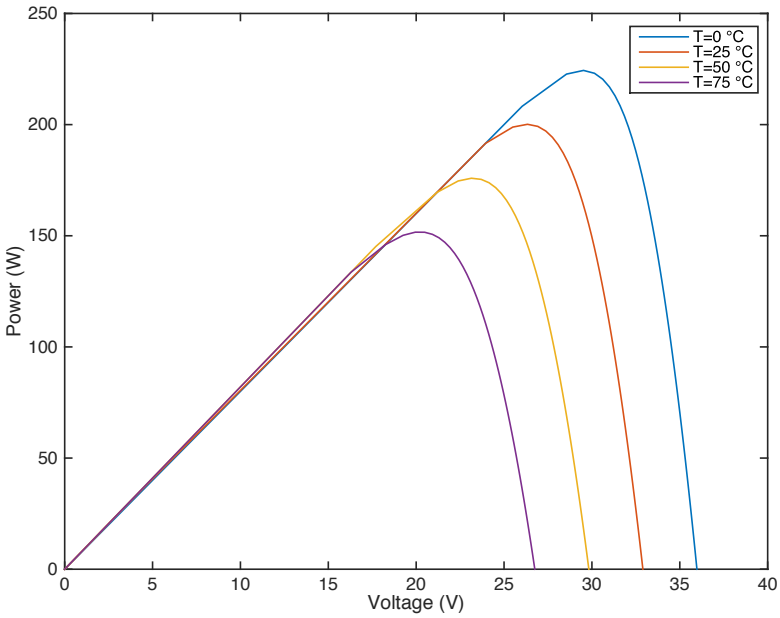

Figure 4.6 *Power-Voltage characteristic of KC200GT (polycrystalline) PV module at different temperatures and standard irradiance.*

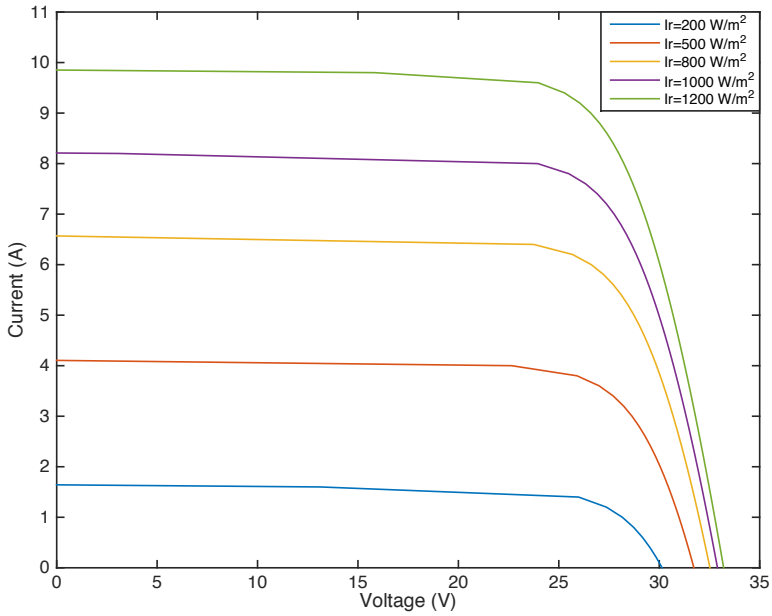

Figure 4.7 *Current-Voltage characteristic of KC200GT (polycrystalline) PV module at different irradiances and standard temperature.*

The I – V and P – V characteristics of polycrystalline silicon PV module at various irradiances are provided in Figure 4.7 and Figure 4.8. The short circuit current is exactly

proportional to insolation. For example, doubling the irradiance will also double the short circuit current. When the irradiance is 500 W/m^2, the short circuit current is 4.105 A, and it changes into 8.21 A when the irradiance is 1000 W/m^2. Meanwhile, the open circuit voltage slightly increases with the increase in insolation at high irradiance levels and more at low irradiance levels, since it is the logarithmic function of irradiance.

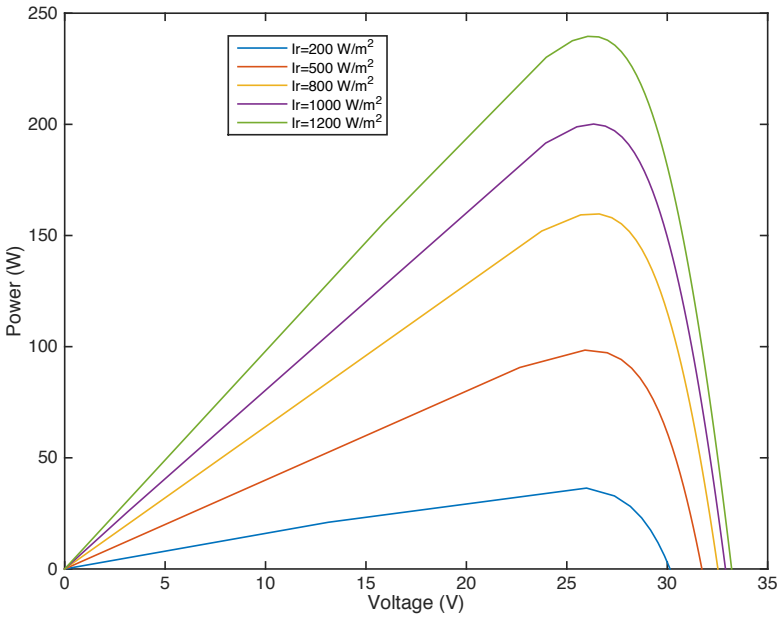

Figure 4.8 *Power-Voltage characteristic of KC200GT (polycrystalline) PV module at different irradiances and standard temperature.*

Figure 4.8 shows that output power increases as irradiance increases, and the maximum power is 200 W when the irradiance is 1000 W/m^2, which is same as the value in the datasheet.

4.2 Simulation results of thin film PV modules

CdTe and CIGS thin film PV modules are also simulated by the single-diode model, while the I – V and P – V curves of amorphous silicon PV module have been obtained by the enhanced single-diode model, which is introduced in Subchapter 3.2.1.

4.2.1 Simulation results of CdTe thin film PV module

The useful parameters of CdTe thin film PV module Calyxo CX3 in the simulation are shown in Table 4.3 [23], which is from Calyxo GmbH.

Table 4.3 *Input data of Calyxo CX3 (CdTe) PV module to the model.*

Parameter	Value	Parameter	Value
V_{oc}	62 V	k_v	-148.8 mV/℃
I_{sc}	1.95 A	k_i	0.39 mA/℃
V_{mpp}	46.3 V	R_{sh}	554.8 Ω
I_{mpp}	1.65 A	R_s	1.7249 Ω
P_{mpp}	75 W	A	1.5

The effect of temperature on I – V characteristic of CdTe thin film PV module is verified in Figure 4.9. The short circuit current, open circuit voltage and maximum power at 25 ℃ are consistent with the datasheet values. For example, when the temperatures are 25 ℃ and 50 ℃, the respective open circuit voltages are 62 V and 58.28 V, and short circuit currents are 1.95 A and 1.96 A. So the calculated temperature coefficients are -148.8 mV/℃ and 0.4 mA/℃, which are almost same as the values given in the datasheet.

Figure 4.10 presents the P – V characteristic of CdTe thin film PV module at different temperatures and standard irradiance. The power output decreases significantly when the temperature increases.

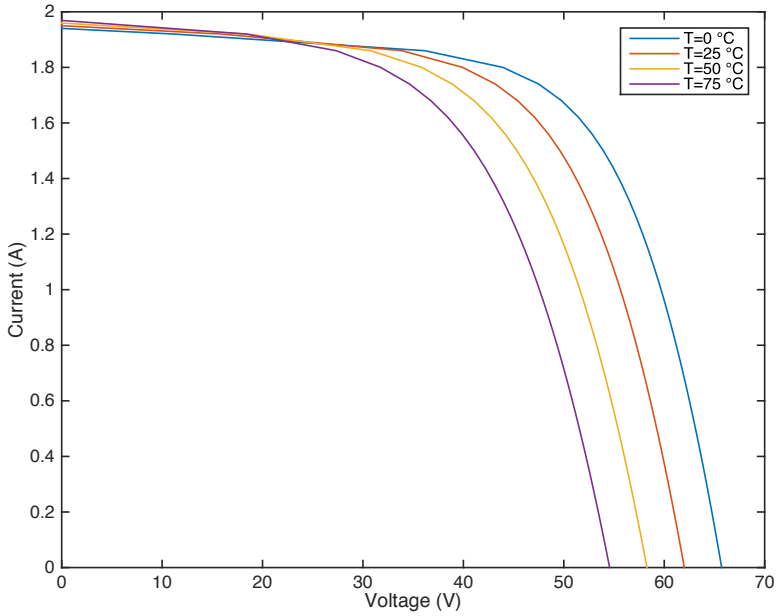

Figure 4.9 *Current-Voltage characteristic of Calyxo CX3 (CdTe) PV module at different temperatures and standard irradiance.*

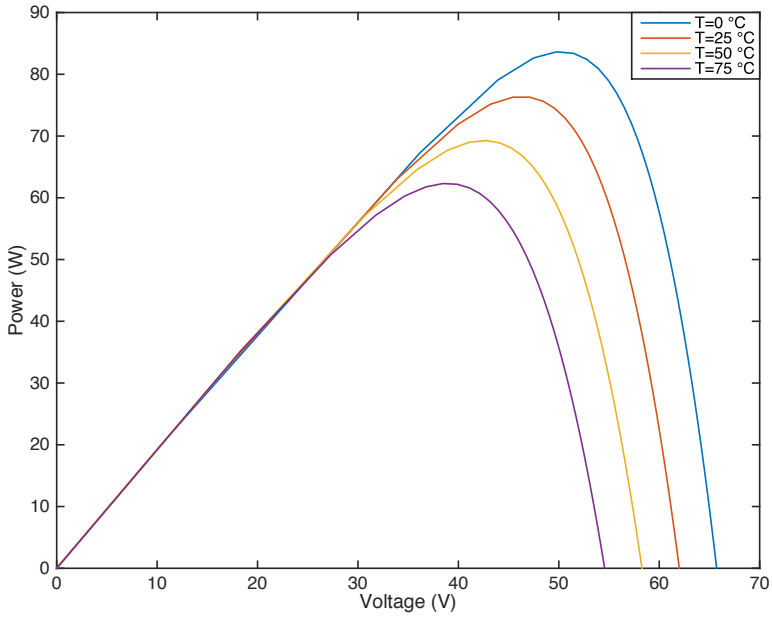

Figure 4.10 *Power-Voltage characteristic of Calyxo CX3 (CdTe) PV module at different temperatures and standard irradiance.*

Figures 4.11 and 4.12 give the I – V and P – V characteristics of CdTe thin film PV module at five different irradiances when the temperature is 25 ℃.

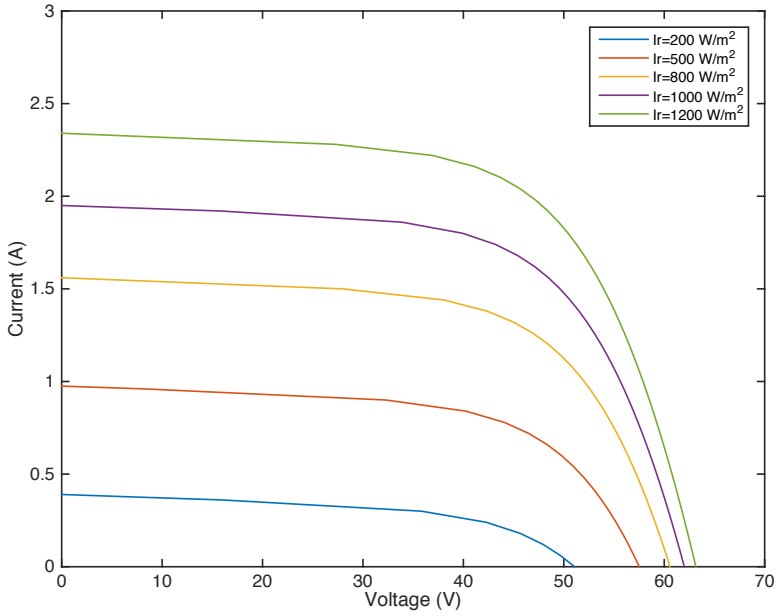

Figure 4.11 *Current-Voltage characteristic of Calyxo CX3 (CdTe) PV module at different irradiances and standard temperature.*

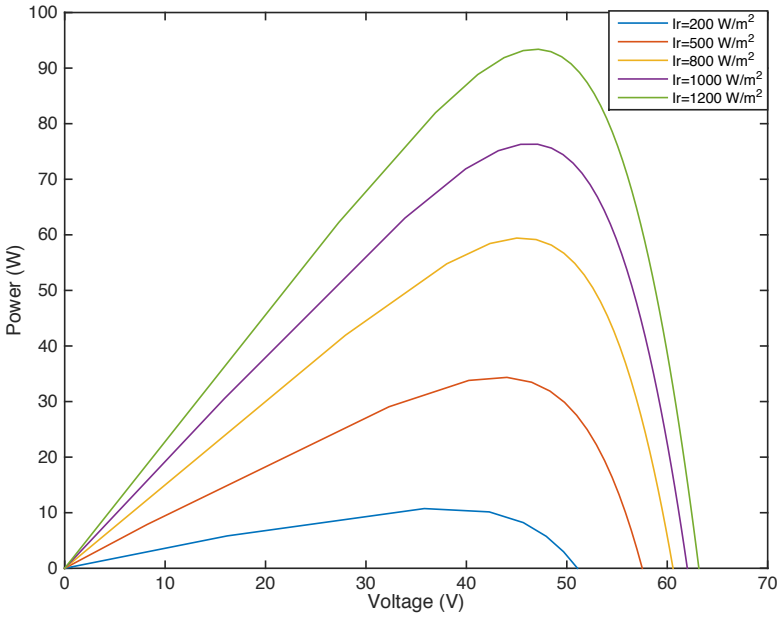

Figure 4.12 *Power-Voltage characteristic of Calyxo CX3 (CdTe) PV module at different irradiances and standard temperature.*

Figure 4.11 shows a linear relationship between the short circuit current and irradiance. It is obvious that when the irradiance increases from 500 W/m^2 to 1000 W/m^2, the short circuit current varies from 0.975 A to 1.95 A. At the same time, Figure 4.12 attests that the open circuit voltage is logarithmically dependent on the irradiance.

4.2.2 Simulation results of CIGS thin film PV module

Table 4.4 shows the datasheet and calculated (R_s and R_{sh}) values of CIGS thin film PV module BIPV-300 from Global Solar Energy Incorporated [24].

Table 4.4 *Input data of BIPV-300 (CIGS) PV module to the model.*

Parameter	Value	Parameter	Value
V_{oc}	71.2 V	k_v	-235 mV/°C
I_{sc}	6.4 A	k_i	-1.92 mA/°C
V_{mpp}	53.9 V	R_{sh}	159.2 Ω
I_{mpp}	5.6 A	R_s	1.1921 Ω
P_{mpp}	300 W	A	1.5

Figure 4.13 and 4.14 show the simulation results for the CIGS thin film PV module under different temperatures with the irradiance at 1000 W/m^2.

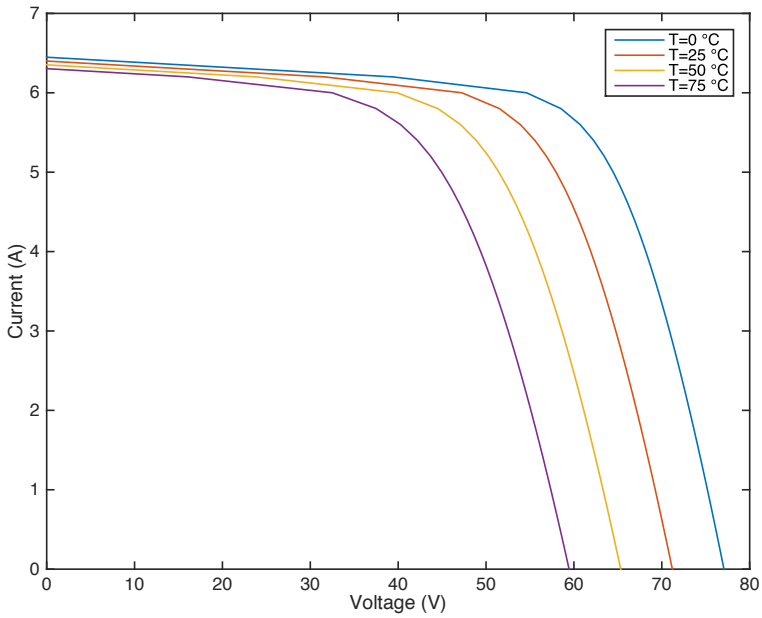

Figure 4.13 *Current-Voltage characteristic of BIPV-300 (CIGS) PV module at different temperatures and standard irradiance.*

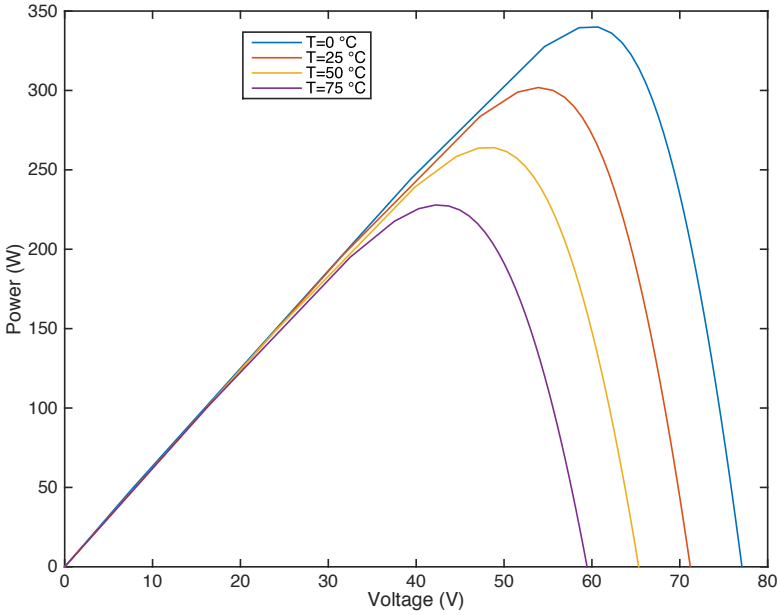

Figure 4.14 *Power-Voltage characteristic of BIPV-300 (CIGS) PV module at different temperatures and standard irradiance.*

The I – V curves of CIGS PV module is a little different from other I – V characteristics. The temperature coefficients of open circuit voltage and short circuit current are all negative, thus both current and voltage decrease with a temperature increase.

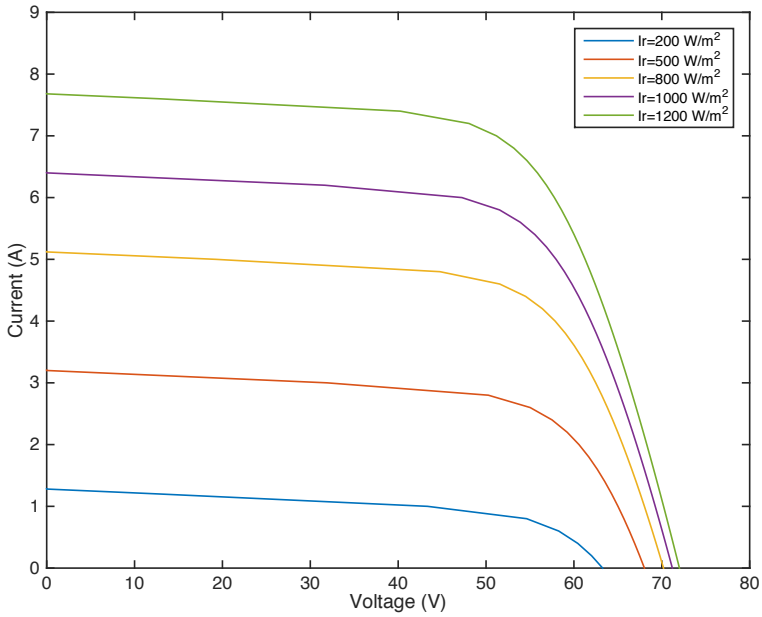

Figure 4.15 *Current-Voltage characteristic of BIPV-300 (CIGS) PV module at different irradiances and standard temperature.*

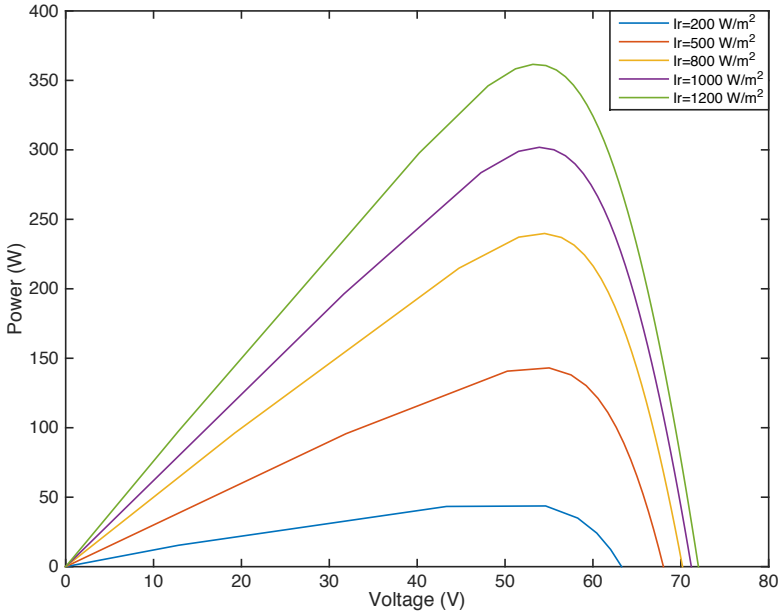

Figure 4.16 *Power-Voltage characteristic of BIPV-300 (CIGS) PV module at different irradiances and standard temperature.*

Figure 4.15 and 4.16 show the I – V and P – V characteristics of CIGS thin film PV module with the changing irradiance and fixed temperature at 25℃. The curves indicate the effects of irradiance on the current is more obvious than the effects of temperature while the influences of irradiance on the voltage are not as apparent as the temperature influence.

4.2.3 Simulation results of a-Si PV module

Table 4.5 summarizes the useful parameters of amorphous silicon PV module SCHOTT ASI™ 95 from SCHOTT Solar AG in simulating [25].

Table 4.5 *Input data of SCHOTT ASI™ 95 (a-Si) PV module to the model.*

Parameter	Value	Parameter	Value
V_{oc}	23.6 V	k_v	-77.9 mV/℃
I_{sc}	6.69 A	k_i	5.35 mA/℃
V_{mpp}	17.4 V	R_{sh}	61.4 Ω
I_{mpp}	5.47 A	R_s	0.0514 Ω
P_{mpp}	95.18 W	A	2

The operation results of the amorphous silicon PV module under different conditions are shown in Figure 4.17 to Figure 4.20.

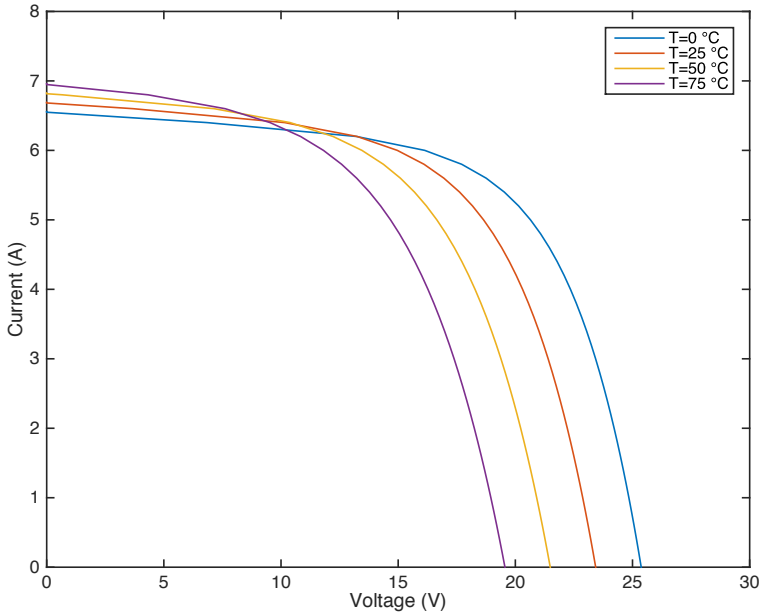

Figure 4.17 *Current-Voltage characteristic of SCHOTT ASI™ 95 (a-Si) PV module at different temperatures and standard irradiance.*

Figure 4.17 shows the I – V characteristic of amorphous silicon PV module at different temperatures and standard irradiance. The short circuit current is significantly larger than the current at the maximum power point, which can also be verified by the datasheet in Table 4.5. The difference of short circuit current and maximum power point current is 1.22 A, while the difference for the monocrystalline silicon PV module is only 0.37 A. It will be reflected on the fill factor and PV module efficiency. Similarly, the changes in short circuit current and open circuit voltage are in agreement with the temperature coefficients. In the curves of 0 ℃ and 25 ℃, the short circuit currents are 6.549 A and 6.683 A, while the open circuit voltages are 25.37 V and 23.43 V. Thus, the temperature coefficients are 5.36 mA/℃ and -77.6 mV/℃, which are almost same as the values provided in the datasheet.

The P – V characteristic of amorphous silicon PV module with various temperatures and standard irradiance is provided in Figure 4.18. The power output has a significant reduction as the temperature rises.

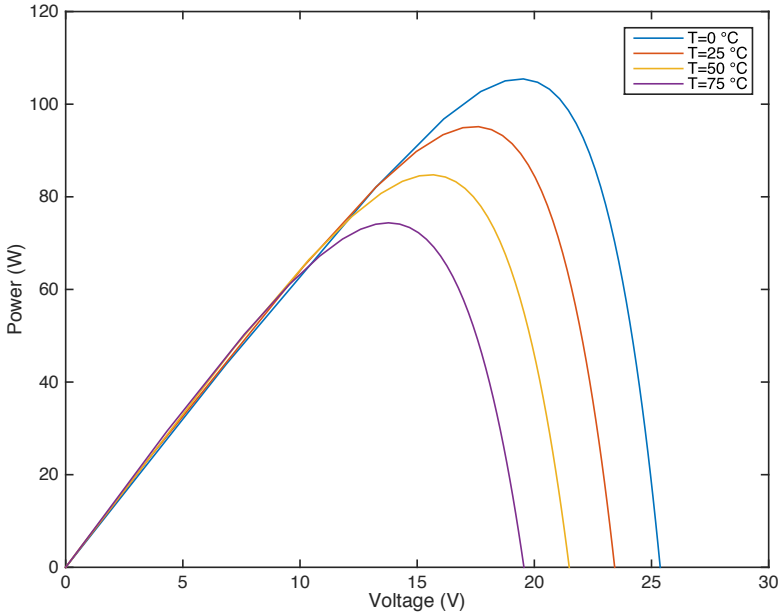

Figure 4.18 *Power-Voltage characteristic of SCHOTT ASI™ 95 (a-Si) PV module at different temperatures and standard irradiance.*

Figures 4.19 and 4.20 show how the irradiance changes affect the voltage, current and power output supplied by the PV module under a constant temperature condition. With the irradiance value increases, the short circuit current also increases linearly but open circuit voltage increases logarithmically. Meanwhile, the maximum power increases with the increasing irradiance, and the value at 1000 W/m^2 is 95.15 W, almost equals to the

maximum power provided by the manufacturer in the datasheet.

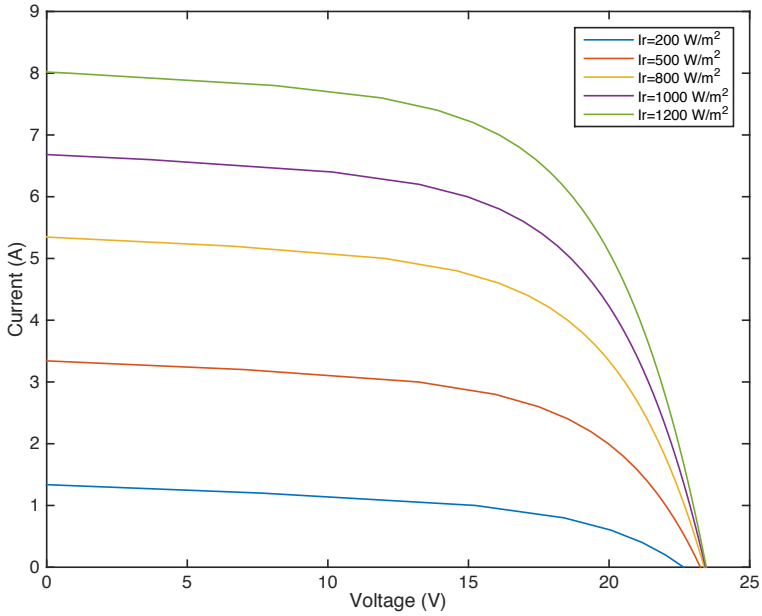

Figure 4.19 *Current-Voltage characteristic of SCHOTT ASI™ 95 (a-Si) PV module at different irradiances and standard temperature.*

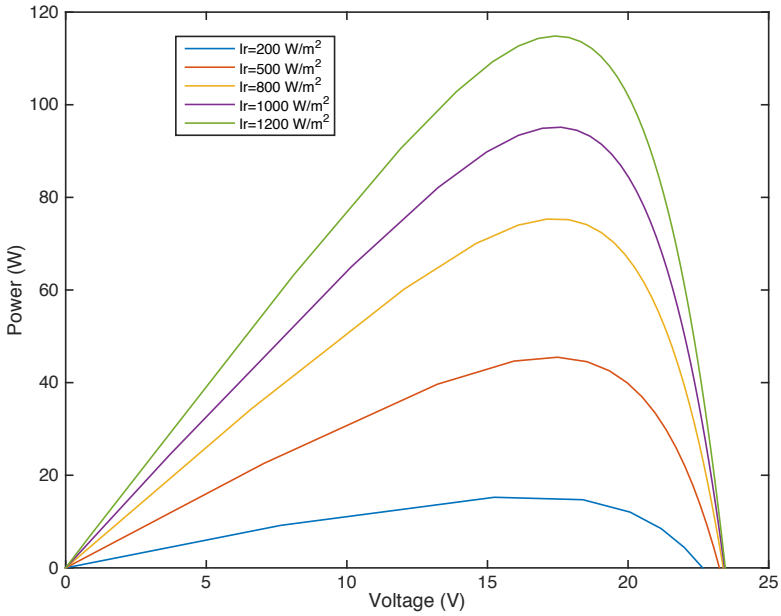

Figure 4.20 *Power-Voltage characteristic of SCHOTT ASI™ 95 (a-Si) PV module at different irradiances and standard temperature.*

5. EVALUATION OF THE PHOTOVOLTAIC MODULES

There are five different types of photovoltaic modules which are made out of different materials. This chapter gives a comparison of their features according to the datasheets and curves of current-voltage and power- voltage in different conditions obtained in Chapter 4. The modules will be managed from four perspectives: fill factor, PV module efficiency, power warranty and PV module stability. The stability can be analyzed from two conditions: variation of maximum power at different temperature levels and constant insolation (1000 W/m^2), and variation of maximum power at different insolation levels and constant temperature (25 ℃).

Fill factor (FF), a measure of collecting carriers capacity as a function of voltage, is the ratio of the maximum power P_{mpp} to the product of the open circuit voltage V_{OC} and short circuit current I_{SC}, which can be expressed as $\mathrm{FF} = \frac{V_{mpp} \cdot I_{mpp}}{V_{OC} \cdot I_{SC}}$. Graphically, the fill factor is the area ratio of A and B, so $\mathrm{FF} = \frac{\mathrm{A}}{\mathrm{B}}$. Figure 5.1 (a) indicates the PV module with high fill factor, and Figure. 1 (b) is the PV module with low fill factor. It is obvious that the more "square" shaped the area A is, the larger is the FF value of a PV module [26].

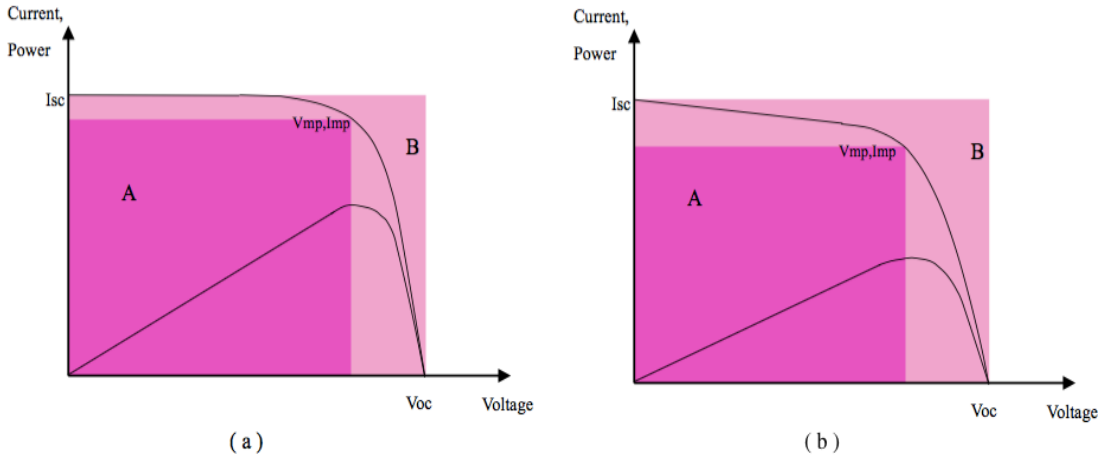

Figure 5.1 *Illustration of the fill factor.*

PV module efficiency η_{PV} is the ratio of maximum power P_{mpp} to the radiation power arriving at the PV module, thus it is closely related to the PV module area, A_Z, and irradiance *G*. The efficiency of PV modules is a significant index that determines the annual energy output of the system. Power warranty, which is guaranteed by the producers, can be obtained from product datasheets. Finally, the maximum powers in different conditions can be collected through the curves of Chapter 4.

5.1 Crystalline Silicon PV modules

5.1.1 Monocrystalline silicon PV module

The fill factor of monocrystalline silicon PV module from SunPower Corporation is

$$\mathrm{FF} = \frac{P_{mpp}}{V_{OC} \cdot I_{SC}} = \frac{345\ \mathrm{W}}{68.2\ \mathrm{V} \cdot 6.39\ \mathrm{A}} = 0.792$$

The equation concludes that the fill factor will change with the different environment conditions, due to the variation of the maximum power, open circuit voltage and short circuit current.

The PV module efficiency is calculated under standard test condition (STC), so $\mathrm{G} = 1000\ \mathrm{W/m^2}$.

$$\eta_{PV} = \frac{P_{mpp}}{G \cdot A_Z} = \frac{345\ \mathrm{W}}{1000\ \mathrm{W/m^2} \cdot (1.559\ \mathrm{m} \cdot 1.046\ \mathrm{m})} = 0.212$$

Monocrystalline silicon PV modules have the highest PV module efficiency, which is about 15 – 20 %. As a result, the monocrystalline silicon PV modules are space-efficient, they generate electricity up to four times compared to thin film PV modules. Nevertheless, monocrystalline silicon PV modules are the most expensive PV module, and the whole circuit could break down if just a part of the PV module is covered by snow, shade or dirt.

Module power warranty can be presented as Power output – Years figure. Figure 5.2 shows the power warranty of monocrystalline silicon PV modules. SunPower offers the best power warranty compared to other traditional photovoltaic modules: 95 % for first 5 five years and -0.4 % per year to year 25 [21].

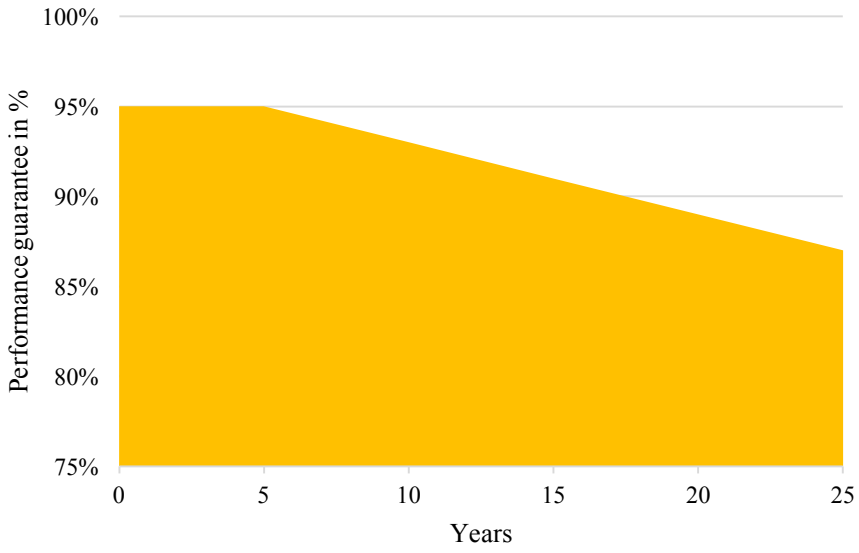

Figure 5.2 *Power warranty of X21-345 (monocrystalline) PV module.*

The figures of Power – Voltage characteristics give the maximum powers at different temperature levels and constant insolation (1000 W/m²), and then the variation curves can be provided. Table 5.1 list the maximum powers which decrease from 369.4 W to 294.4 W while the temperature rises from 0 ℃ to 75 ℃. The reduction ratio is 20.35 %. At the same time, the broken-line graph is given according to the data.

Table 5.1 *Maximum Power temperature dependence of X21-345 (monocrystalline) PV module.*

Temperature (℃)	Maximum Power (W)
0	369.4
25	345
50	319.9
75	294.4
Change of Power	-20.35%

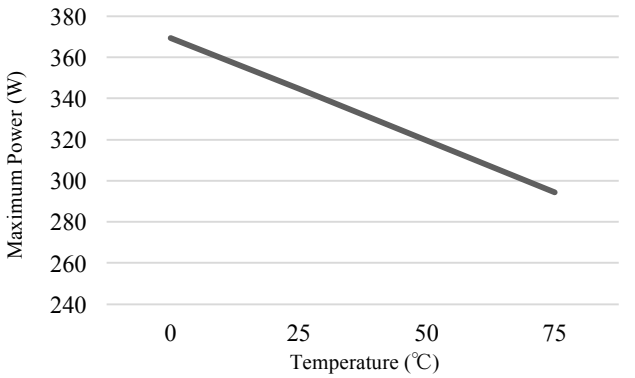

Similarly, the maximum powers can also be read from the P – V figures of fixed temperature (25 ℃) and different irradiances. The maximum powers at different irradiances are listed in Table 5.2. The powers increase 563.31 % with the irradiances increase from 200 W/m² to 1200 W/m². The corresponding broken-line graph is presented on the right side.

Table 5.2 *Maximum Power irradiance dependence of X21-345 (monocrystalline) PV module.*

Irradiance (W/m^2)	Maximum Power (W)
200	62.61
500	168
800	274.2
1000	344.9
1200	415.3
Change of Power	563.31%

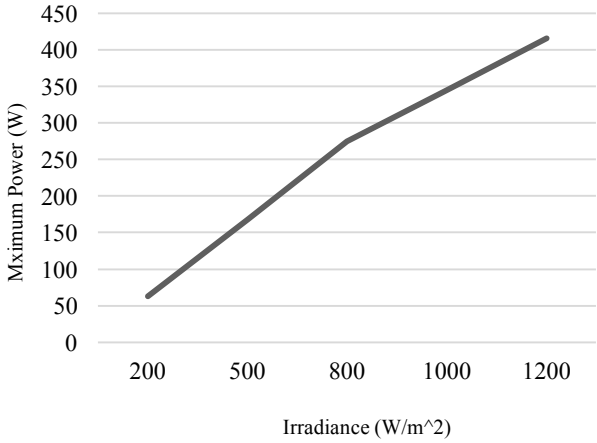

5.1.2 Polycrystalline silicon PV module

The fill factor of polycrystalline silicon PV module from Kyocera Corporation is

$$\mathrm{FF} = \frac{P_{mpp}}{V_{OC} \cdot I_{SC}} = \frac{200\ \mathrm{W}}{32.9\ \mathrm{V} \cdot 8.21\ \mathrm{A}} = 0.74$$

The PV module efficiency is

$$\eta_{PV} = \frac{P_{mpp}}{G \cdot A_Z} = \frac{200\ \mathrm{W}}{1000\ \mathrm{W/m^2} \cdot (1.425\ \mathrm{m} \cdot 0.99\ \mathrm{m})} = 0.142$$

which is lower than X21-345 monocrystalline silicon PV module because of the lower silicon purity. The PV module efficiency of polycrystalline silicon PV module is about 13 – 16 %, which has been an excellent result while still lagging behind the efficiency achieved by monocrystalline silicon PV module. Therefore, the space-efficiency is also lower and it requires a larger area to generate the same electricity compared to monocrystalline silicon PV module.

Figure 5.3 gives the power warranty of polycrystalline silicon PV module. The warrant of power output is always lower than for the monocrystalline PV module produced by SunPower Corporation. Long term output warranty shall warrant if PV module exhibits power output of less than 90 % of the original minimum rated power within 10 years and less than 80 % within 20 years [22]. It is a traditional warranty, rather than the warranty of power output decreasing every year like X21-345 PV module.

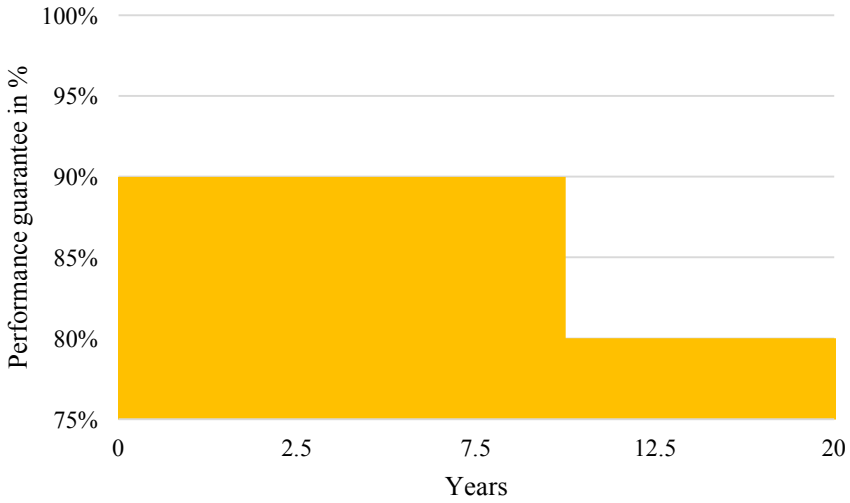

Figure 5.3 *Power warranty of KC200GT (polycrystalline) PV module.*

Table 5.3 and Table 5.4 give the changes of maximum power with the temperature and irradiation, the variation curves are also provided respectively at the same time. It is obvious that the change tendency is similar as monocrystalline silicon PV module, just the maximum power reduced pace with varying temperature of KC200GT polycrystalline silicon PV module is faster than X21-345 monocrystalline silicon PV module, thus, the KC200GT is more sensitive to temperature than X21-345.

Table 5.3 *Maximum Power temperature dependence of KC200GT (polycrystalline) PV module.*

Temperature (℃)	Maximum Power (W)
0	224.4
25	200.1
50	175.9
75	151.6
Change of Power	-32.44%

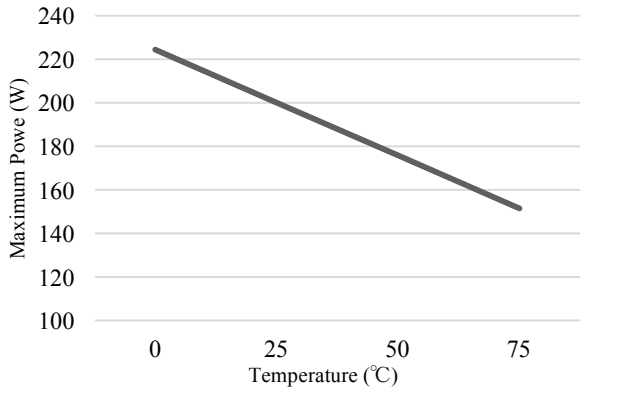

The maximum power increase from 36.38 W to 239.6 W with the raise of irradiance from 200 W/m^2 to 1200 W/m^2, the growth rate is 558.6 %, which is approximately equal to the growth rate of monocrystalline silicon PV module.

Table 5.4 *Maximum Power irradiance dependence of KC200GT (polycrystalline) PV module.*

Irradiance (W/m^2)	Maximum Power (W)
200	36.38
500	98.44
800	159.7
1000	200.1
1200	239.6
Change of Power	558.6%

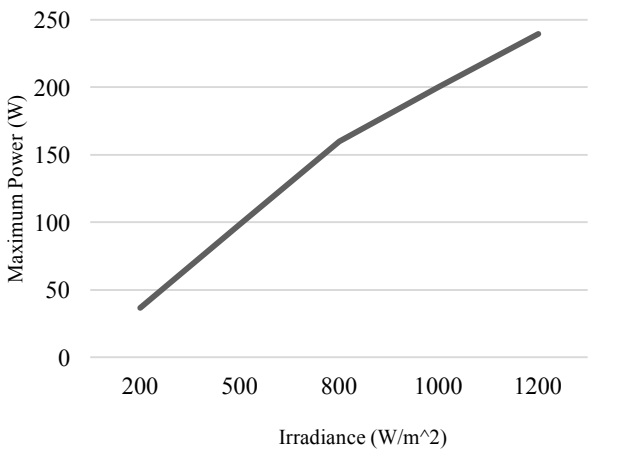

5.2 Thin film PV modules

5.2.1 CdTe thin film PV module

The fill factor of CdTe thin film PV module Calyxo CX3 is

$$\mathrm{FF} = \frac{P_{mpp}}{V_{OC} \cdot I_{SC}} = \frac{75\ \mathrm{W}}{62\ \mathrm{V} \cdot 1.95\ \mathrm{A}} = 0.62$$

The PV module efficiency of Calyxo CX3 can be written as

$$\eta_{PV} = \frac{P_{mpp}}{G \cdot A_Z} = \frac{75\ \mathrm{W}}{1000\ \mathrm{W/m^2} \cdot (1.2\ \mathrm{m} \cdot 0.6\ \mathrm{m})} = 0.132$$

The power warranty of Calyxo CX3 in Figure 5.4 is same as KC200GT: 90 % the initial efficiency up to 10 years and 80 % up to 25 years [23].

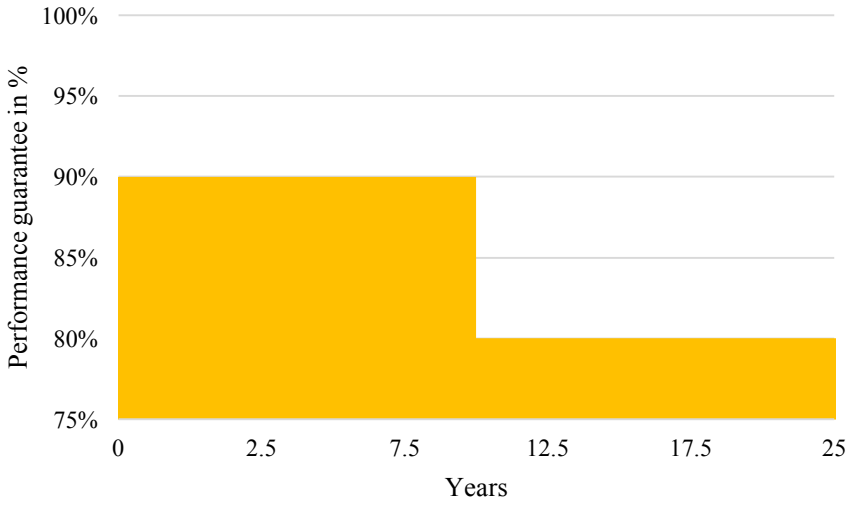

Figure 5.4 *Power warranty of Calyxo CX3 (CdTe) PV module.*

Table 5.5 and Table 5.6 provide the maximum power variation of CdTe thin film PV module Calyxo CX3 under different temperature and irradiance. When the temperature changes from 0 ℃ to 75 ℃, the maximum power decreases from 83.64 W to 62.3 W, and the reduction is 25.51 %.

Table 5.5 *Maximum Power temperature dependence of Calyxo CX3 (CdTe) PV module.*

Temperature (℃)	Maximum Power (W)
0	83.64
25	76.3
50	69.27
75	62.3
Change of Power	-25.51%

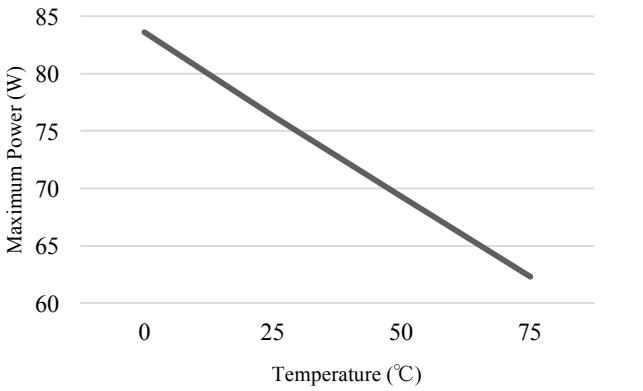

The growth of maximum power when irradiance increases from 200 W/m² to 1200 W/m² is 821.19 %, apparently higher than the growth of crystalline silicon PV modules. As a consequence, the CdTe thin film PV module is more sensitive to irradiation than crystalline silicon PV modules.

Table 5.6 *Maximum Power irradiance dependence of Calyxo CX3 (CdTe) PV module.*

Irradiance (W/m^2)	Maximum Power (W)
200	9.783
500	32.21
800	56.64
1000	73.39
1200	90.12
Change of Power	821.19%

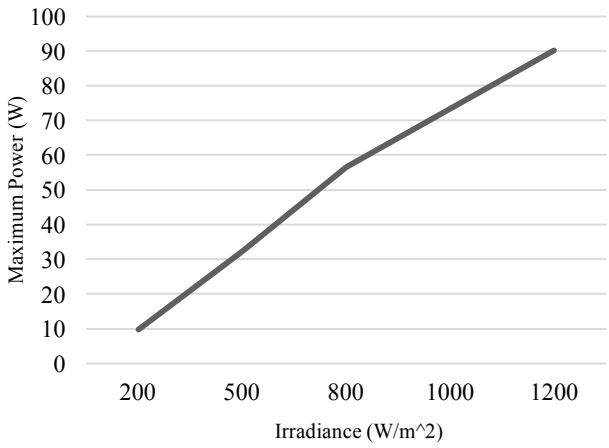

5.2.2 CIGS thin film PV module

CIGS thin film PV module is made of the alloy of copper, indium, gallium and selenium. Thus, it is not influenced by the shortage of silicon supply. The fill factor of CIGS thin film PV module BIPV-300 is calculated as

$$\mathrm{FF} = \frac{P_{mpp}}{V_{OC} \cdot I_{SC}} = \frac{300\ \mathrm{W}}{71.2\ \mathrm{V} \cdot 6.4\ \mathrm{A}} = 0.658$$

The PV module efficiency is defined as below. The record laboratory efficiency of CIGS thin film PV module is still lower than 20 %.

$$\eta_{PV} = \frac{P_{mpp}}{G \cdot A_Z} = \frac{300\ \mathrm{W}}{1000\ \mathrm{W/m^2} \cdot (5.745\ \mathrm{m} \cdot 0.495\ \mathrm{m})} = 0.105$$

The power output is warranted 25 years as in Figure 5.5, 90 % of the initial efficiency in first 10 years and 80 % in following 15 years [24].

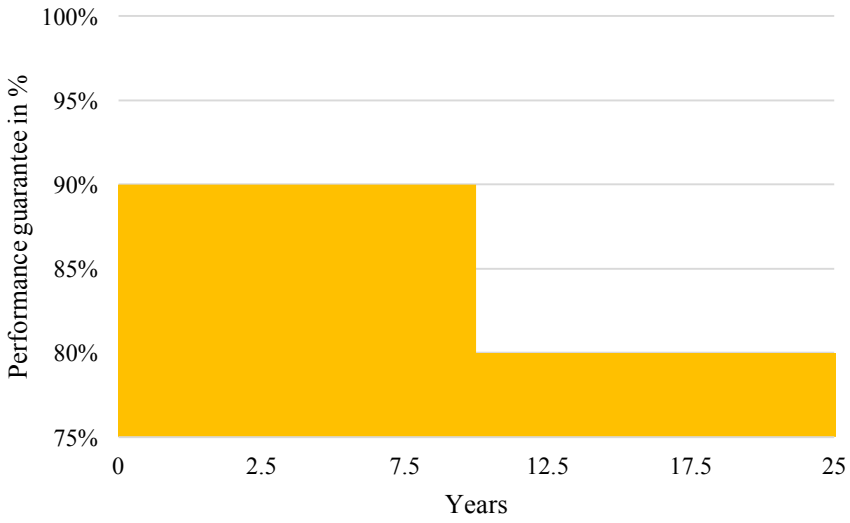

Figure 5.5 *Power warranty of BIPV-300 (CIGS) PV module.*

Table 5.7 and Table 5.8 present the maximum powers of CIGS thin film PV module at different temperatures and irradiances. The CIGS thin film PV module is sensitive to both temperature and irradiation. The maximum power changes from 339.9 W to 227.9 W when the temperature varies from 0 to 75 centigrade, the reduction is 32.95 %, more sensitive to temperature than CdTe thin film PV module.

Table 5.7 *Maximum Power temperature dependence of Calyxo BIPV-300 (CIGS) PV module.*

Temperature (℃)	Maximum Power (W)
0	339.9
25	301.8
50	264
75	227.9
Change of Power	-32.95%

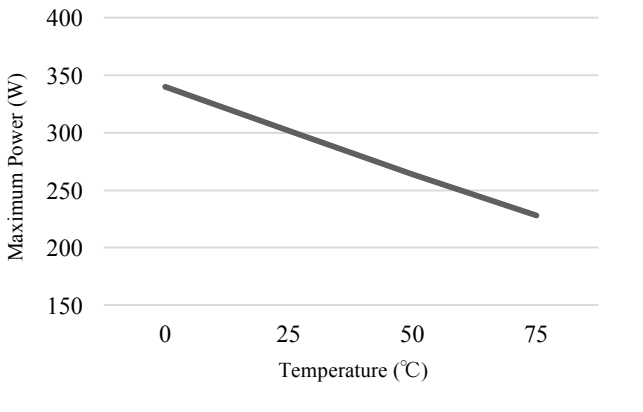

The maximum power increases 317.8 W when the irradiance changes from 200 W/m^2 to 1200 W/m^2, the power variation is 727.23 %. Therefore, CIGS thin film PV module is also more sensitive to irradiation than crystalline silicon PV module.

Table 5.8 *Maximum Power irradiance dependence of Calyxo BIPV-300 (CIGS) PV module.*

Irradiance (W/m^2)	Maximum Power (W)
200	43.7
500	143
800	239.8
1000	301.8
1200	361.5
Change of Power	727.23%

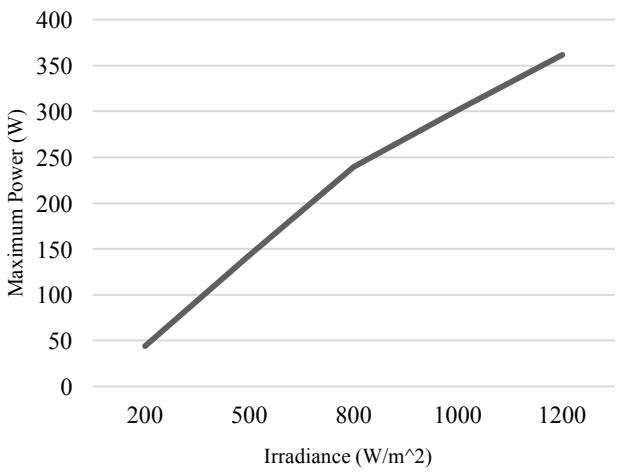

5.2.3 a-Si PV module

Amorphous silicon PV module fill factor is smaller than for former PV modules.

$$\mathrm{FF} = \frac{P_{mpp}}{V_{OC} \cdot I_{SC}} = \frac{95\ \mathrm{W}}{23.6\ \mathrm{V} \cdot 6.69\ \mathrm{A}} = 0.602$$

The PV module efficiency of amorphous silicon PV module SCHOTT ASI 95 is obtained as follows, it is also much lower than for the previous PV modules.

$$\eta_{PV} = \frac{P_{mpp}}{G \cdot A_Z} = \frac{95\ \mathrm{W}}{1000\ \mathrm{W/m^2} \cdot (1.108\ \mathrm{m} \cdot 1.308\ \mathrm{m})} = 0.066$$

SCHOTT Solar supports its product ASI 95 with a linear warranty as shown in Figure 5.6. It is guaranteed that the power output will be more than 97 % of initial for the first year, and reduction will be no greater than 0.7 % per year for years 2 to 25 [27]. Meanwhile, it is promised the output will be at least 90.7 % after 10 years, and at least 80.2 % output after 25 years [27]. Comparing with the other thin film PV modules, the power warranty of amorphous silicon PV module is better than for CdTe and CIGS PV modules in each period.

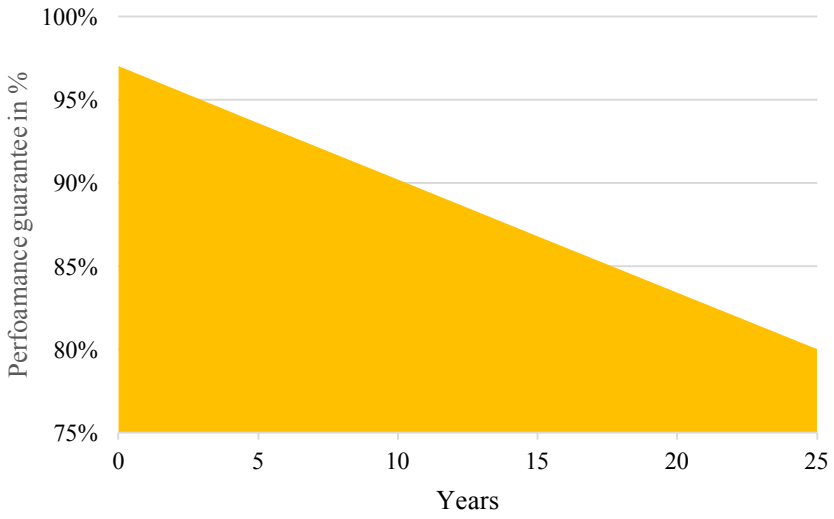

Figure 5.6 *Power warranty of SCHOTT ASI 95 (a-Si) PV module.*

Table 5.9 and Table 5.10 give the maximum power variation of amorphous silicon PV module at different temperatures and irradiances. When the temperature rises from 0 ℃ to 75 ℃, the maximum power decreases from 89.67 W to 61.56 W, the reduction is 31.35%.

Table 5.9 *Maximum Power temperature dependence of SCHOTT ASI 95 (a-Si) PV module.*

Temperature (℃)	Maximum Power (W)
0	89.67
25	79.82
50	70.36
75	61.56
Change of Power	-31.35%

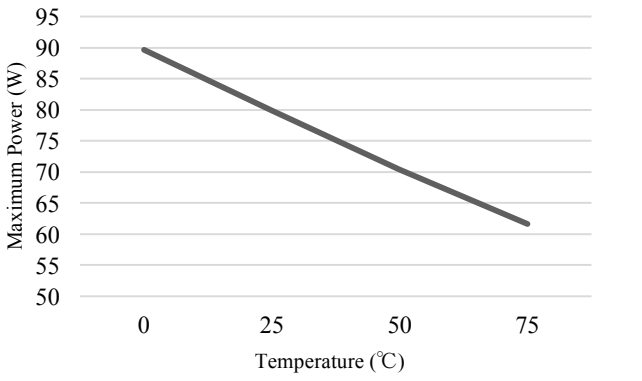

Conversely, the maximum power increases with the irradiance raises, the growth rate of maximum power is 651.25 %. Although the irradiation sensitivity of amorphous silicon PV module is not as high as for CdTe and CIGS thin film PV modules, it is also more sensitive to irradiation than crystalline silicon PV modules.

Table 5.10 *Maximum Power irradiance dependence of SCHOTT ASI 95 (a-Si) PV module.*

Irradiance (W/m^2)	Maximum Power (W)
200	12.82
500	38.16
800	63.21
1000	79.82
1200	96.31
Change of Power	651.25%

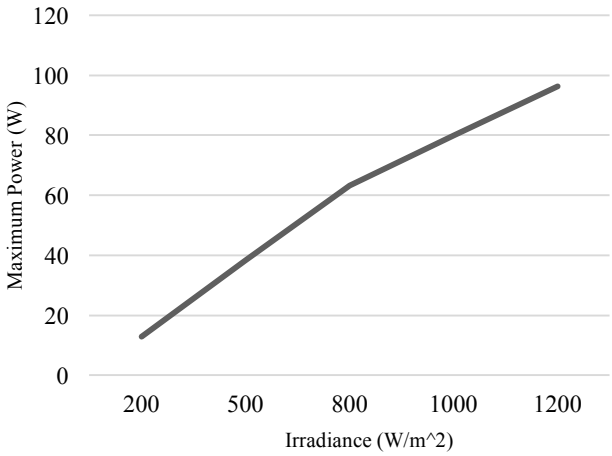

5.3 Comparison of Characteristics

Figure 5.7 summarizes the identical characteristics of different PV modules, including fill factor, PV module efficiency, rate of change of maximum power at different temperature and irradiance.

According to the Figure 5.7 (a), monocrystalline silicon PV module has the largest fill factor, as a result, it is the best product to collect carriers in a cell. In Figure 5.7 (b), monocrystalline silicon PV module is the most efficient product with the greatest stability, since its variance ratio is small (Figure 5.7 (c) and (d)). However, the cost of producing monocrystalline silicon PV module is so high, thus, it is not an economical choice. As a consequence, although the fill factor and PV module efficiency of polycrystalline silicon PV module are a bit lower than for monocrystalline silicon PV module, it still dominates the market of PV modules. The Sunpower's monocrystalline silicon PV module produces around triple the electricity with the same amount of space compared with amorphous silicon PV module. Low efficiency means they need more space to install more hardware to produce same power output as crystalline silicon PV modules. Moreover, amorphous silicon is cheaper than crystalline silicon PV modules, since it is a direct-bandgap material and just need about 1 % silicon to make of the crystalline silicon-based PV module, as well as the substrates can be produced by inexpensive materials like glass and plastic, instead of silicon [28].

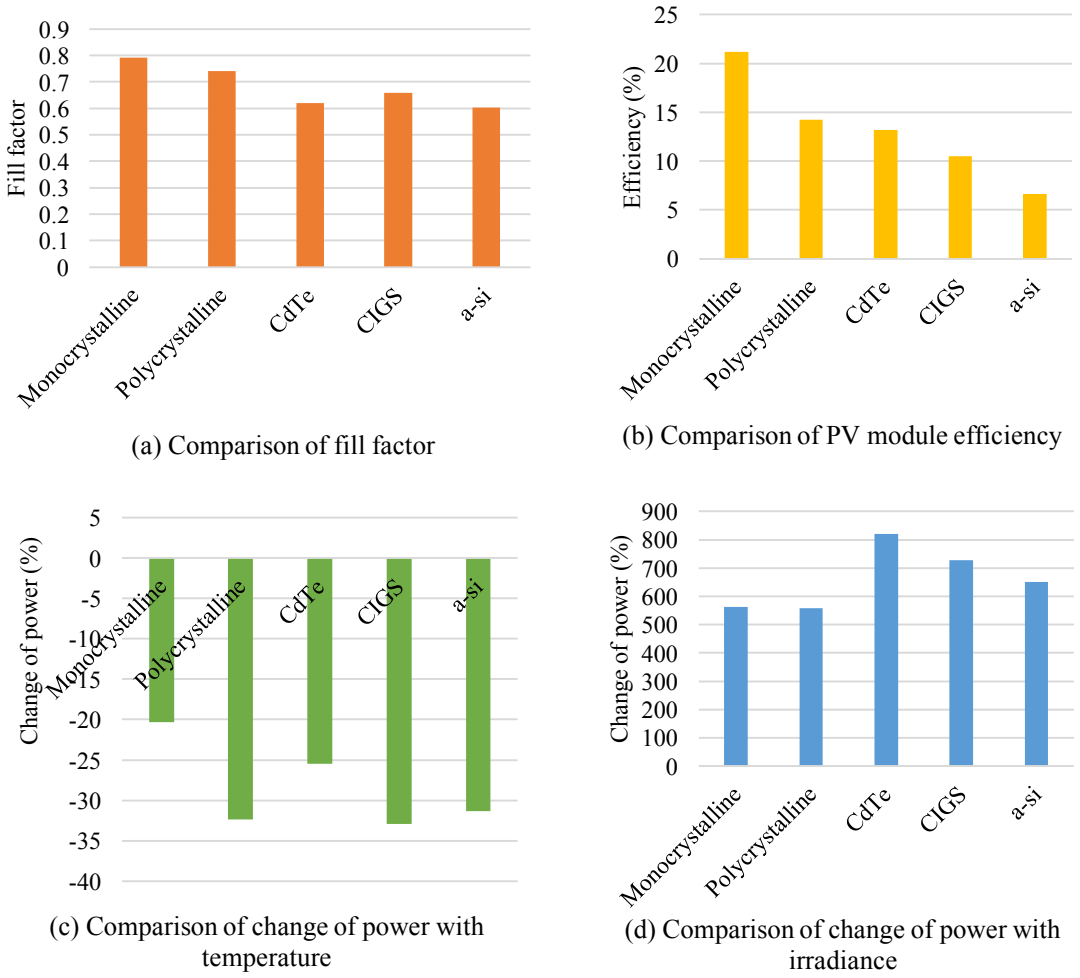

Figure 5.7 *Comparison characteristics of different PV modules*

According to Figure 5.7 (c) and (d), thin film materials are not as stable as crystalline silicon PV modules, in other words, the power output change distinctly with the variation of temperature and irradiance, subsequently leading to degradation over time. On one hand, the maximum power decreases when the temperature increases from 0 ℃ to 75 ℃, and the reduction of monocrystalline silicon PV module is smallest. Therefore, the monocrystalline silicon PV module X21-345 from SunPower Corporation has the best stability when temperature changes. On the other hand, the maximum power increases when the irradiance changes from 200 W/m^2 to 1200 W/m^2. It is apparent in Figure 5.7 (d) that the three thin film PV modules are more sensitive to irradiance than crystalline silicon PV modules. The power growth rate of thin film PV modules is larger than 650%, however, as for crystalline silicon PV modules, the power growth rate is smaller than 600% when irradiance increases from 200 W/m^2 to 1200 W/m^2.

Taking into account all factors, the mono- and polycrystalline silicon PV module is a good

choice for residential home who have limited space. By contrast, thin film PV modules are applicable to people who have enough space and want to spend less. They are flexible so that they can be installed on curved surfaces where this is not a viable option for crystalline silicon PV modules. Meanwhile, thin film PV module is suited to the mobile user like vehicles since they are lightweight.

6. CONCLUSION

Solar power is a renewable and environmental friendly energy. It is developing quickly and will be an important type of important renewable energy to replace the fossil fuels. PV module is the core of a solar power system, and the technologies of PV modules have matured and became popular after the development of over 170 years.

The main objective of this thesis was to compare the commercial solar photovoltaic modules made by various materials from different companies. The five different photovoltaic (PV) modules were studied through four aspects: the fill factor and PV module efficiency at Standard Test Condition (STC), maximum power at changing temperature and standard irradiance, and maximum power at various irradiance and constant temperature. The last two properties were researched by using Matlab Simulink model. They used the single-diode five-parameters model except for amorphous silicon PV modules, which used enhanced single-diode model, with an additional current sink.

The method of extracting the five parameters according to the manufacturers' datasheets was provided, and the obtained values were used in the Simulink model. The Simulink models were operated under various temperatures and irradiances. The simulation results, which were shown by Current – Voltage and Power – Voltage curves, were in accordance with expectations: at the condition of constant irradiance and various temperature, the variation of open circuit voltage and short circuit current coincided with the temperature coefficients; and at the situation of different irradiance with standard temperature, the short circuit currents were linearly dependent with the irradiance, while open circuit voltages were logarithmically dependent on the irradiance.

In addition, the fill factor and PV module efficiency of these PV modules were compared at STC. Monocrystalline silicon PV module is the most efficient product with the best capacity of collecting carriers. As for the power warranty, monocrystalline silicon PV module is also the best one among all PV products. After monocrystalline silicon PV module, polycrystalline silicon PV module is the second best PV product considering the four aspects, and it is cheaper than the former.

This thesis presents a comprehensive comparison of five PV modules made by different materials and companies based on the manufacturers' datasheets and simulation results. The advantages and disadvantages were revealed. However, these studies are theoretical analysis. In order to verify the conclusion, the current and voltage at different temperature and irradiance should be measured on the real PV modules. Then the I – V and P – V curves can be plotted and the fill factor and PV module efficiency in a natural environmental condition can be calculated. On the one hand, the practical performance of these PV modules can be discovered in the experiment. On the other hand, the availability of both single-diode model and enhanced single-diode model can be demonstrated. This would be an interesting continuation of the thesis.

REFERENCES

[1] D. Sera, R. Teodorescu, P. Rodriguez, PV panel model based on datasheet values, Industrial electronics, Jun 2007, pp. 2392-2396.

[2] "2014 Key World Energy Statistics" (PDF). Available at: http://www.iea.org/publications/freepublications/.

[3] Renewable energy statistics. Available at: http://ec.europa.eu/eurostat/statistics-explained/index.php/Renewable_energy_statistics.

[4] The history of solar. Available at: https://www1.eere.energy.gov/solar/pdfs/solar_timeline.pdf.

[5] Photovoltaic (PV) cells. Available at: http://www.altenergy.org/renewables/photovoltaic-cells.html.

[6] Photovoltaic cell, module, string, array. Available at: https://www.homepower.com/view/?file=HP113_pg106_WordPower.

[7] Photovoltaic modules. Available at: http://www.sunlightelectric.com/pvmodules.php.

[8] S. R. Wenham, M. A. Green, M. E. Watt., R. Corkish, Applied Photovoltaics, Earthscan, 2007, Chapt. 2.

[9] M. R. Abdelkader, A. Al-Salaymeh, Z. Al-Hamamre, Firas Sharaf, A comparative analysis of the performance of monocrystalline and multicrystalline PV cells in Semi Arid Climate Conditions: the case of Jordan, Jordan journal of mechanical and industrial engineering, vol. 4, Nov 2010.

[10] U.S. Department of Energy, Sunshot vision study, Feb 2012.

[11] L. A. Dobrzanski, M. Szczesna, M. Szindler, A. Drygata, Electrical properties mono- and polycrystalline silicon solar cells, Journal of achieveents in materials and manufacturing engineering, vol. 59, Aug 2013.

[12] Solar electric photovoltaic modules. Available at: http://www.solardirect.com/pv/pvlist/pvlist.htm.

[13] M. Prorok, B. Werner, T. Zdanowicz, Applicability of equivalent diode models to modeling various thin-film photovoltaic (PV) modules in a wide range of temperature and irradiance conditions, Electron technology internet journal, vol. 37/38, Nov 2006.

[14] M. A. E. H. Mohamed, M. H. Osman, Evaluation of a PV model based on a novel parameter estimation procedure for different manufacturers modules, International journal of engineering research & technology, vol. 3, Jan 2014, pp. 971 – 977.

[15] A. Dandoussou, M. Kamta, L. Bitjoka, P. Wira, A. Kuitché, Simulations based on experimental data of the behavior of a monocrystalline silicon photovoltaic module, Journal of solar energy, vol. 2015, Aug 2015.

[16] A. Gupta, V. U. Srinivasa, Design, simulation and verification of generalized photovoltaic cells model using first principles modeling, ACEEE International journal on control system and instrumentation, vol. 03, no. 01, Feb 2012, pp. 11 – 17.

[17] G. Petrone, G. Spagnuolo, Parameters identification of the single-diode model for amorphous photovoltaic panels, 2015 International Conference on Clean Electrical Power (ICCEP), Jun 2015, pp. 105 – 109.

[18] S. Nonomura, H. Okamoto, Y. Haakawa, Determination of the built-in potential in a-Si solar cells by means of electroabsorption method, Japanese journal of applied physics, vol. 21, 1982, pp. L464 – L466.

[19] M. T. Boyd, S. A. Klein, D. T. Reindl, B. P. Dougherty, Evaluation and validation of equivalent circuit photovoltaic solar cell performance models, Journal of solar energy engineering, vol. 133, no. 2, Mar 2011, pp. 1 – 13.

[20] R. Kind, R. A. C. M.M. van Swaaij, F. A. Rubinelli, S. Solntsev, M. Zeman, Thermal ideality factor of hydrogenated amorphous silicon p-i-n solar cells, Journal of applied physics, vol. 110, Nov 2011.

[21] SunPower X21-345 solar panel datasheet. Available at: http://us.sunpower.com/sites/sunpower/files/media-library/data-sheets/ds-x21-series-335-345-residential-solar-panels.pdf.

[22] Kyocera KC200GT solar panel datasheet. Available at: http://www.kyocerasolar.com/assets/001/5195.pdf.

[23] Calyxo CX3 solar panel datasheet. Available at: http://energiaslnka.sk/doc/fotovoltaika/hybrid/specifikacia/datenblatt%20CX3%20eng_85.pdf.

[24] Global Solar BIPV solar panel datasheet. Available at: http://www.gruppocastiglioni.com/baenergie/pdf/PowerFLEX_6m.pdf.

[25] SCHOTT ASI™ solar panel datasheet. Available at: http://www.comel.gr/pdf/schottsolar/ASI95-97-100-103.pdf.

[26] B. J. Modtland, Improving the light-induced degradation of hydrogenated amorphous silicon solar cells using fabrication at elevated temperatures and low pressure, Iowa State University, 2013.

[27] Linear performance warranty. Available at: https://www.civicsolar.com/sites/default/files/documents/schott-solar-warranty-brochure-us-0811-56576.pdf.

[28] M. A. Maehlum, Amorphous silicon solar panels, Energy Informative, Jun 2013. Available at: http://energyinformative.org/amorphous-silicon-solar-panels/.